sults suggest that HuR regulates the translation of *ARF* mRNA, we next sought to determine if HuR associates with *ARF* mRNA. Wild-type MEFs were infected with control (GFP) or HA-HuR expression retroviruses, and HA-HuR complexes were immunoprecipitated using HA antibody. As previously reported, β-*actin*, c-*myc*, and *p53* mRNAs were specifically enriched in HuR complexes (Fig. 7A) (16, 20, 26). Under these conditions, we could not detect *ARF* mRNA in the HuR immune complex. We performed similar experiments with endogenous HuR proteins and failed to detect binding of HuR to *ARF* mRNA (Fig. 7B). We next employed a UV cross-linking and immunoprecipitation (CLIP) assay, which is a more sensitive method to detect protein-RNA interaction. MEFs were irradiated with UV to covalently cross-link protein-RNA complexes prior to lysate preparation and immunoprecipitated using HuR or control antibodies. Although we could not detect the HuR and *ARF* mRNA interaction with the standard RNA immunoprecipitation protocol (Fig. 7A and B), *ARF* mRNA was slightly enriched in HuR immune complexes following UV cross-linking (Fig. 7C). Hence, it is likely that *ARF* mRNAs form an extremely fragile or transient complex in living cells, unlike other HuR ligands.

HuR regulates the translation of ARF mRNA through its 5′UTR. To find the region responsible for HuR in *ARF* mRNA, we expressed exogenous *ARF* mRNA that included the open reading frame (ORF) and both the 5′- and 3′UTRs (full-length *ARF*), the ORF and 5′UTR (Δ3′UTR *ARF*), or the ORF and 3′UTR (Δ5′UTR *ARF*) in NIH 3T3 cells (*ARF* and *Ink4a* null) expressing sh-SCR or sh-HuR. These cells expressed comparable amounts of exogenous *ARF* mRNA (Fig. 8A). Under these conditions, $p19^{ARF}$ levels were increased in the absence of HuR expression, and this effect was more prominent in full-length *ARF* mRNA cells and in Δ3′UTR cells than in Δ5′UTR cells (Fig. 8B). $p19^{ARF}$ expression from Δ5′UTR *ARF* mRNA was also slightly increased in HuR-depleted cells. However, this likely reflects the larger amount of *ARF* mRNA in these cells (Fig. 8A), since the effect of HuR knockdown was diminished when $p19^{ARF}$ levels were normalized to *ARF* mRNA levels in each sample (Fig. 8C). Consistently with the above results, we observed more ribosome association with full-length and Δ3′UTR *ARF* mRNAs than with Δ5′UTR mRNA in the absence of HuR (Fig. 8D). Furthermore, CLIP analysis revealed that the 5′UTR is required for HuR association (Fig. 8E). Together, these results strongly suggest that HuR regulates the translation of *ARF* mRNA through its 5′UTR. Consistently with this notion, *ARF* mRNA localized to nucleoli irrespective of HuR status when the 5′UTR was deleted (Fig. 6B, lowest panels). However, this region by itself did not respond to HuR when it was conjugated to the luciferase reporter (data not shown), suggesting that the ORF region also contributes to regulation or that there are more-stringent requirements for the RNA secondary structure. We also performed similar experiments using full-length *Ink4a* mRNA or *Ink4a* mRNA lacking both the 5′ and 3′UTRs (ORF). Consistently with the above results indicating that HuR does not increase $p16^{Ink4a}$ levels in MEFs and that *ARF* mRNA does not share the 5′UTR with *Ink4a*, knockdown of HuR did not affect $p16^{Ink4a}$ expression from these mRNAs, further confirming that the effect of HuR is specific to *ARF* in this locus (Fig. 9).

Nucleolin interacts with ARF mRNA in nucleoli and is required for $p19^{ARF}$ expression in HuR knockdown cells. We next sought a possible mediator of $p19^{ARF}$ expression in HuR knockdown cells. The nucleolar RNA-binding protein nucleolin has

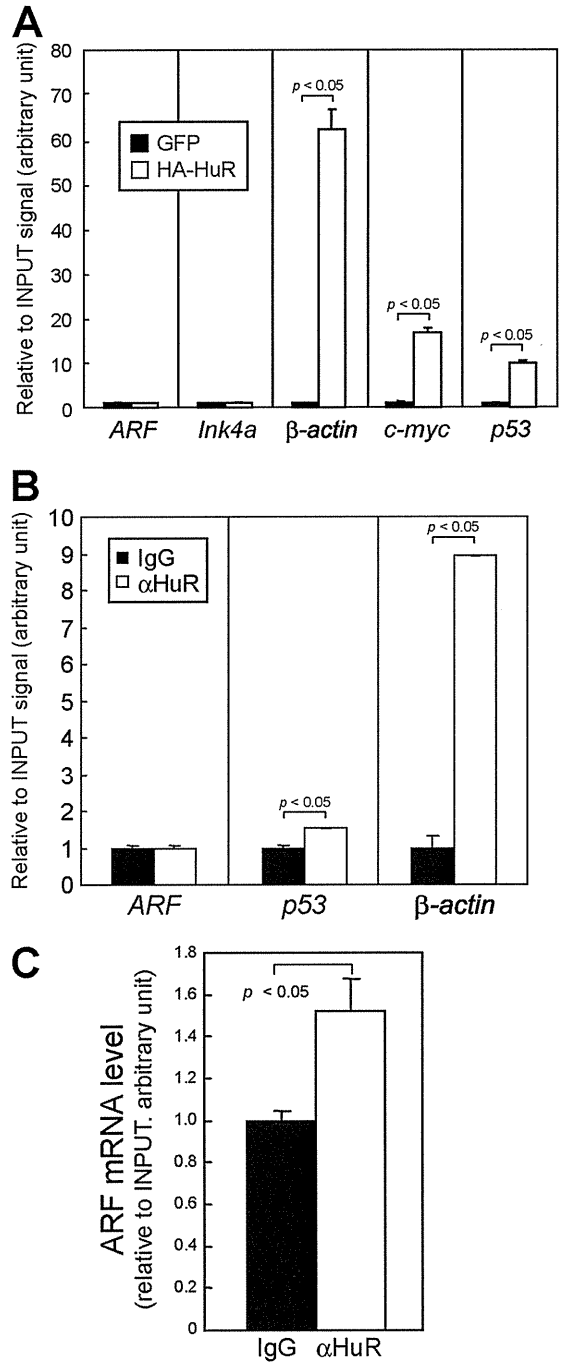

FIG 7 HuR weakly associates with *ARF* mRNA in living cells. (A) Lysates of (wild-type) MEFs expressing HA-tagged HuR proteins were immunoprecipitated using HA antibody. RNA extracted from the immune complex was analyzed by real-time PCR. Error bars represent SEM ($n = 3$). (B) Lysates prepared from wild-type MEFs were immunoprecipitated using control (IgG) or HuR antibodies. RNAs were extracted from immune complexes and subjected to real-time PCR analysis. *p53*, c-*myc*, and β-*actin* were used as positive controls. (C) Lysates were prepared from UV-cross-linked MEFs and immunoprecipitated using control or HuR antibodies. RNAs were recovered from the immune complex following proteinase K treatment and analyzed by real-time PCR for *ARF* mRNA levels. Error bars represent SEM of results from triplicate samples.

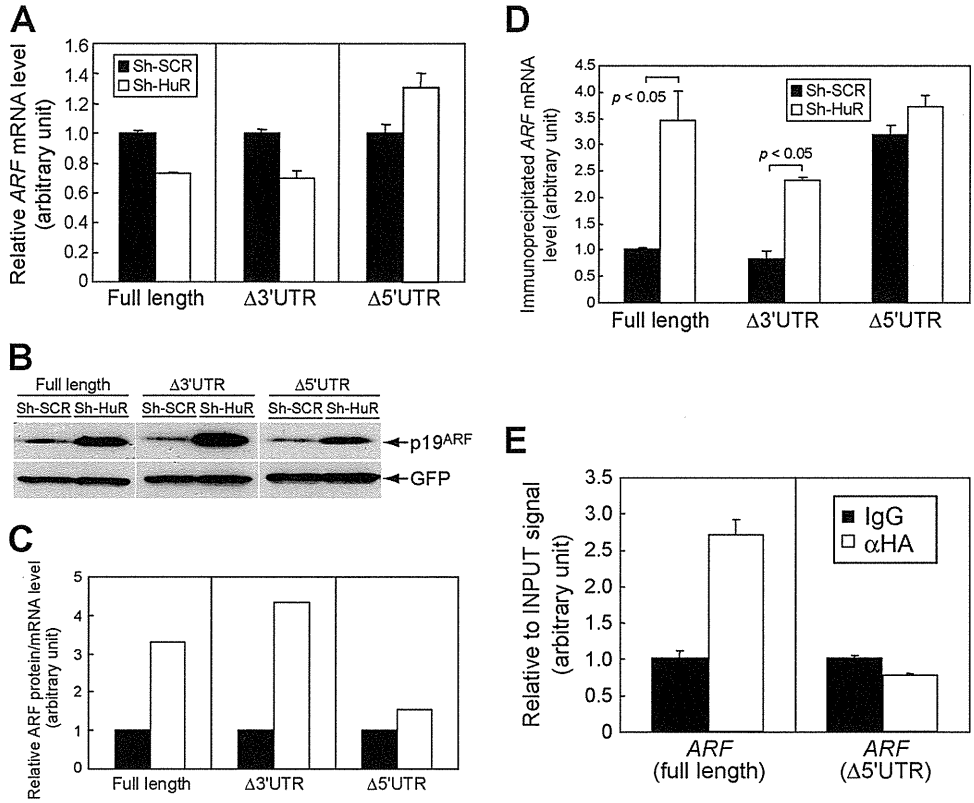

FIG 8 HuR regulates p19^{ARF} expression through the 5′UTR of *ARF* mRNA. (A) NIH 3T3 cells expressing sh-SCR or sh-HuR were transfected with plasmids bearing full-length *ARF*, including the 5′- and 3′UTRs (full length), *ARF* lacking the 3′UTR (Δ3′UTR), or *ARF* lacking the 5′UTR (Δ5′UTR) together with GFP expression plasmids. Three days later, total RNA was extracted and exogenous *ARF* expression was analyzed by real-time PCR. Values were normalized to *GFP* mRNA levels in each sample. (B) The cells from panel A were analyzed by immunoblotting for expression of p19^{ARF} and GFP. (C) p19^{ARF} levels in panel B were quantified using ImageJ, and the p19^{ARF} level and *ARF* mRNA level in each sample were calculated. (D) NIH 3T3 cells expressing sh-SCR or sh-HuR were transfected with *ARF* expression plasmids (full length, Δ3′UTR, or Δ5′UTR) together with GFP-L10 plasmids. Three days later, cytoplasmic lysates were prepared and immunoprecipitated using GFP antibody to purify RNA-protein complexes, including GFP-L10. RNAs were recovered from immune complexes and subjected to real-time PCR analysis for *ARF* mRNA. Values were normalized to input signals in each sample. (E) 293T cells were transfected with *ARF* expression plasmids that express full-length or mutant *ARF* mRNA that lacks the 5′UTR (Δ5′UTR) together with HA-HuR expression plasmids. Forty-eight hours later, cells were subjected to UV cross-linking and immunoprecipitated using control or HA antibodies. Recovered RNA was analyzed by real-time PCR. Error bars represent SEM of results from triplicate samples.

been shown to bind to several mRNAs involved in the cellular stress response, and the binding of nucleolin enhances the translation of their target mRNAs (45). Moreover, microarray analysis of mRNA in the nucleolin complex has revealed that *CDKN2A* (*Ink4a* and *ARF*) mRNA physically associates with nucleolin in HeLa cells (45). Because *ARF* mRNA localized to nucleoli upon HuR depletion, we tested if nucleolin interacts with the nucleolar *ARF* mRNA in HuR knockdown cells. While no *ARF* mRNA was detected in the nucleolin complex of control cells, it was significantly enriched in the absence of HuR expression (Fig. 10A). The interaction of nucleolin with *ARF* mRNA does not require 5′UTR; therefore, relocalization of *ARF* mRNA to the nucleolus seems sufficient for the interaction (Fig. 10B). Thus, HuR impedes the nucleolar localization of *ARF* mRNA by binding to its 5′UTR, thereby inhibiting the interaction of *ARF* mRNA with nucleolin. Next, we examined whether nucleolin is required for p19^{ARF} expression in HuR knockdown cells. For this purpose, siRNA targeting *nucleolin* mRNA was transfected into sh-SCR- or sh-HuR-expressing MEFs. Although the effect of siRNA on nucleolin level was limited, p19^{ARF} induction was suppressed to basal levels in HuR knockdown cells (Fig. 10C), suggesting that nucleolin is required for p19^{ARF} induction in HuR-depleted cells.

Loss of HuR inhibits adipocytic differentiation in a p19^{ARF}-dependent manner. A recent report by Minamino and colleagues has shown that senescence in adipose tissue results in decreased insulin sensitivity, thereby leading to type 2 diabetes mellitus (46). Hence, we investigated whether HuR-mediated p19^{ARF} regulation had any effect on adipocyte function. To this end, we first tested whether loss of HuR could affect adipocyte differentiation *in vitro*. Wild-type MEFs expressing sh-SCR or sh-HuR were differentiated into adipocytes in the presence of insulin, dexamethasone, and 3-isobutyl-1-methylxanthine (IBMX). Oil Red O staining revealed that HuR depletion suppressed adipocytic differentiation in wild-type MEFs (Fig. 11A). It has been reported that HuR directly binds to *C/EBPβ* mRNA to regulate its expression (47). We therefore checked if HuR depletion affected the expression of genes required for adipocyte differentiation. As shown in Fig. 11B, C/EBPβ expression was slightly diminished in HuR-depleted cells. Nonetheless, levels of expression of its downstream C/EBPα and PPARγ genes were still comparable to those in control cells, suggesting that defects in adipogenesis in the absence of HuR were

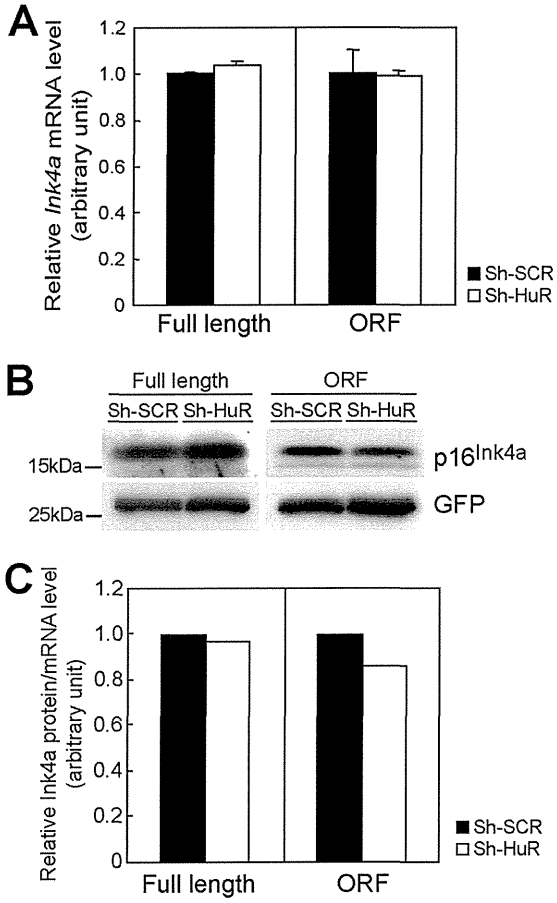

FIG 9 HuR does not affect *Ink4a* translation. (A) NIH 3T3 cells expressing sh-SCR or sh-HuR were transfected with plasmids bearing full-length *Ink4a*, including its 5′- and 3′UTRs (full length), or *Ink4a* lacking its 5′- and 3′UTRs (ORF) together with GFP expression plasmids. Three days later, RNAs were extracted and the expression of exogenous *Ink4a* mRNA was analyzed by real-time PCR. Values were normalized to *GFP* expression levels in each sample. (B) The expression of $p16^{Ink4a}$ and GFP was analyzed by immunoblotting. (C) $p16^{Ink4a}$ levels were quantified and normalized to *Ink4a* expression levels. Error bars represent SEM of results from triplicate samples.

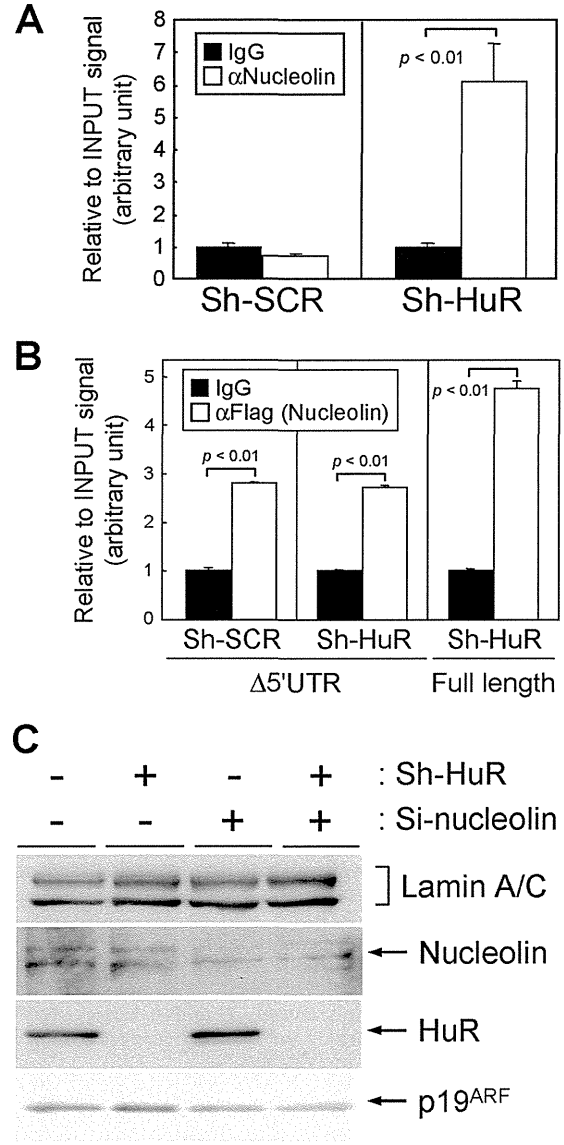

FIG 10 Nucleolin associates with *ARF* mRNA and mediates the $p19^{ARF}$ induction in HuR knockdown cells. (A) Lysates prepared from MEFs expressing sh-SCR or sh-HuR were immunoprecipitated using control (IgG) or nucleolin antibodies. RNAs were recovered from the immune complexes and analyzed by real-time PCR. (B) NIH 3T3 cells expressing sh-SCR or sh-HuR were transiently transfected with *ARF* (Δ5′UTR or full length)-expressing plasmids together with Flag-tagged nucleolin-expressing plasmids. Two days later, lysates were prepared and immunoprecipitated using control or Flag tag (M2) antibodies. RNAs in the immune complexes were analyzed by real-time PCR. Error bars represents SEM of results from triplicate samples. (C) MEFs (P2) expressing sh-SCR or sh-HuR were transfected with siRNA targeting *nucleolin*. Two days later, lysates were prepared and the expression of the indicated proteins was analyzed by immunoblotting. Lamin A/C was used as a loading control.

not attributed to altered expression of adipocyte-related genes. We then checked whether the adipocyte phenotype was dependent on *ARF*. In sharp contrast, HuR knockdown had virtually no effect on adipocyte differentiation in *ARF* knockout MEFs (Fig. 11C).

Given that $p19^{ARF}$ activates the p53-dependent cell cycle checkpoint, we were prompted to check the possibility that $p19^{ARF}$ affects clonal expansion during the initial stage of adipogenesis. Cells were stimulated to differentiate and were pulse-labeled with 5-ethynil-2′-deoxyuridine (EdU) to assess cell cycle reentry. EdU staining showed a significant reduction in cell cycle reentry in HuR-depleted wild-type MEFs (Fig. 11D). In contrast, S-phase entry was not affected by sh-HuR in the absence of *ARF* (Fig. 11E). These results suggest that defective adipogenesis in HuR-depleted cells can be attributed to $p19^{ARF}$-dependent cell cycle arrest or senescence.

Adipose-specific HuR knockout accelerates age-dependent insulin resistance. Our above results indicated that the loss of HuR enhanced the translation of *ARF* mRNA, thus inducing $p19^{ARF}$-dependent cellular senescence, and that HuR may affect adipocyte function through $p19^{ARF}$. To explore the impact of HuR-mediated translational regulation of the *ARF* gene *in vivo*, we generated adipose tissue-specific *HuR* knockout mice ($HuR^{fl/fl}$; AP2-CRE) (Fig. 12A and B) (10). *ARF* mRNA levels were low in the adipose tissue of young animals (1 to 3 months old) of both genotypes but significantly increased in older animals (6 to 9 months old) (Fig. 12C), which is consistent with previous reports

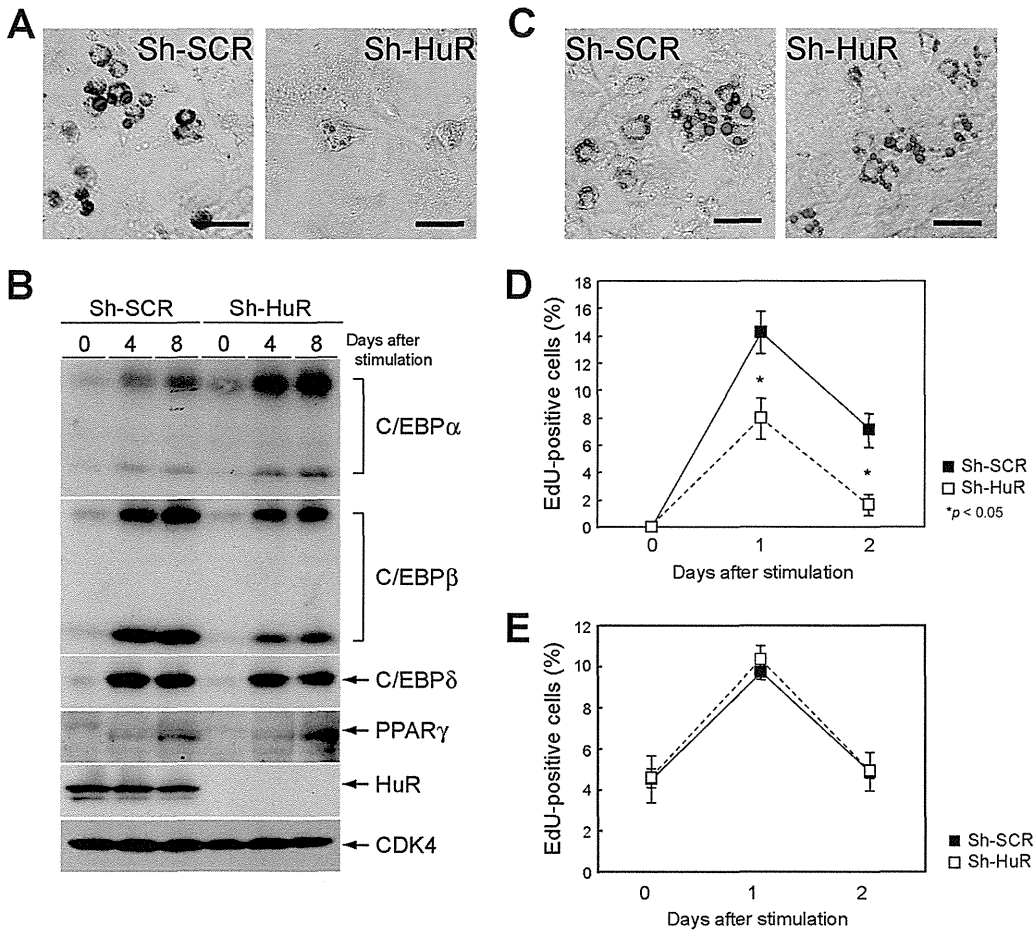

FIG 11 Adipogenesis is impaired in HuR-depleted wild-type MEF. (A) Wild-type MEFs were infected with sh-SCR or sh-HuR retroviruses. Selected cells were stimulated to differentiate them into adipocytes in the presence of insulin, 3-isobutyl-1-methylxanthine (IBMX), and dexamethasone for 10 days and stained with Oil Red O. Bars, 50 μm. (B) Wild-type MEFs with sh-SCR or sh-HuR were cultured in adipocyte differentiation medium for the indicated periods. The expression of C/EBPα, -β, -δ, and PPARγ were analyzed by immunoblotting. (C) *ARF*-null MEFs with sh-SCR or sh-HuR were stimulated to differentiate them for 10 days and stained with Oil Red O. Bars, 50 μm. (D and E) Wild-type (D) and *ARF*-null (E) MEFs expressing sh-SCR or sh-HuR were stimulated to differentiate them for 0, 1, and 2 days. Cells were pulse-labeled with EdU for 45 min and stained for EdU. EdU-positive and -negative cells in microscopic fields were counted. Data are representative of two independent experiments. Error bars represent SEM of results from five microscopic fields.

indicating that *ARF* expression increases in many tissues as animals age (48). $p19^{ARF}$ was still hardly detectable in the adipose tissue of older $HuR^{fl/fl}$ mice (Fig. 12D). However, we detected $p19^{ARF}$ in a certain population of older $HuR^{fl/fl}$; AP2-CRE mouse adipose tissue (Fig. 12E and F). Changes in SA-β-Gal activity were difficult to detect; however, *PAI-1* levels were significantly increased in *HuR* knockout adipose tissue (Fig. 12G). We subsequently tested if HuR loss in adipose tissue affected insulin-mediated glucose homeostasis, which is one of the major functions of this tissue. There was little difference in insulin sensitivity among both genotypes when animals were at a young age; however, in older animals, adipose-specific *HuR* deletion significantly accelerated insulin resistance (Fig. 13A). Similar results were obtained by the glucose tolerance test (Fig. 13B). So far, we have not been able to confirm that this effect is *ARF* dependent, because *ARF*-null animals develop tumors by this age (49). However, the timing of the onset of insulin resistance correlates well with that of $p19^{ARF}$ appearance in adipose tissue. Hence, these results suggest that HuR is required to repress $p19^{ARF}$ expression in adipose tissue, thereby inhibiting adipose senescence, which can lead to insulin resistance.

DISCUSSION

Our data show that HuR is downregulated in senescent mouse fibroblasts and that decreases in HuR contribute to senescence-associated growth arrest. It has been shown that HuR levels decline in human diploid fibroblasts during cellular senescence (22); therefore, the role of HuR in cellular senescence is likely to be evolutionally conserved. How HuR expression is controlled during senescence is unclear, but in human cells, it is attributed, at least in part, to increased expression of miR-519 during senescence (24). Whether HuR is regulated by miRNA in mouse senescence is unknown, but we did not observe a significant change in *HuR* mRNA levels in senescent MEFs (data not shown). Therefore, such posttranscriptional regulation may also contribute to the control of HuR levels in mouse cells.

Although HuR is implicated in senescence in both human and mouse cells, the mechanisms underlying them are different. The

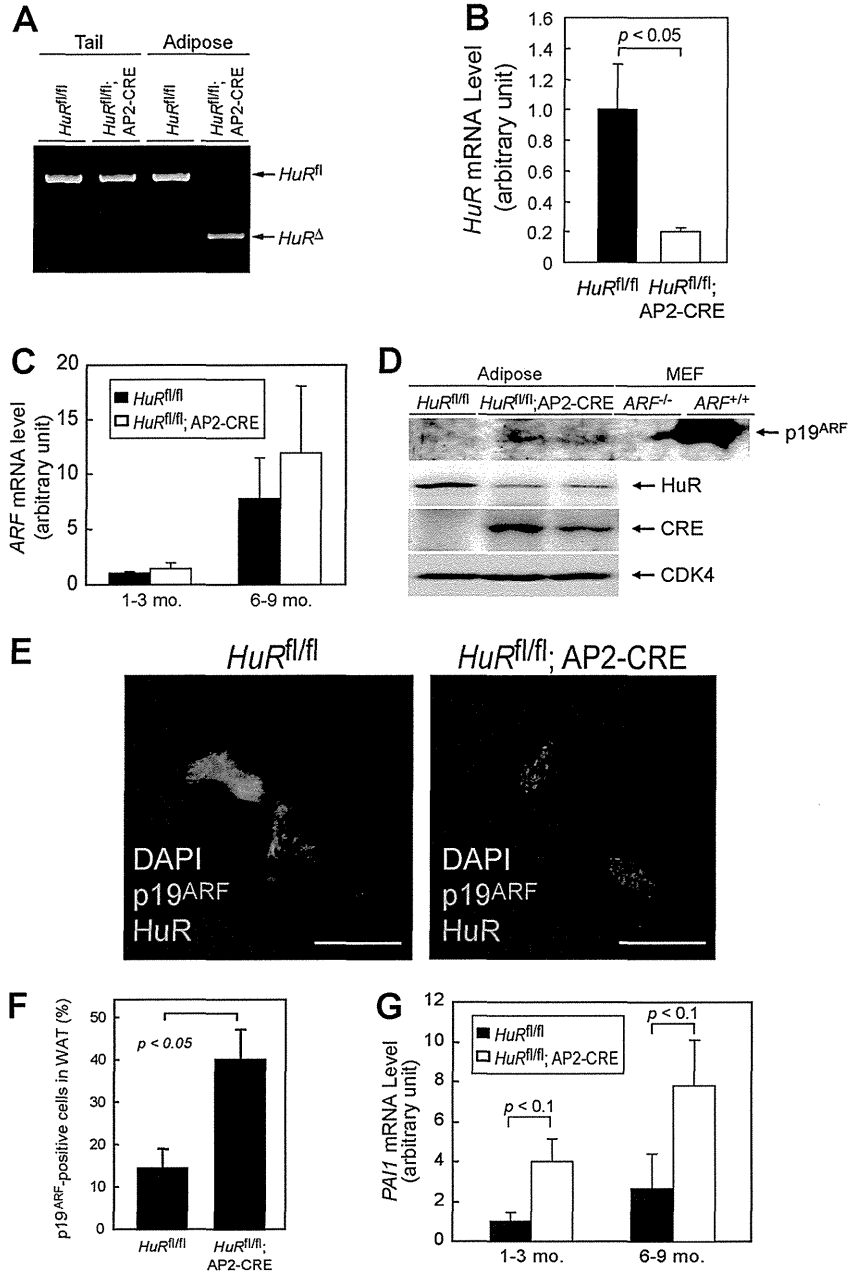

FIG 12 Adipose-specific HuR deletion accelerates the senescence of adipocytes. (A) Genotyping of adipose- and tail-derived genomic DNA. (B) *HuR* mRNA levels in adipose tissue from mice with the indicated genotypes were analyzed by real-time PCR. Values were normalized to 18S rRNA in each sample. (C) *ARF* mRNA was analyzed by real-time PCR. (D) Lysates were prepared from the adipose tissue of $HuR^{fl/fl}$ and $HuR^{fl/fl}$; AP2-CRE mice. Expression of the indicated proteins was analyzed by immunoblotting. CDK4 was used as a loading control. Testis lysate from $ARF^{-/-}$ and $ARF^{+/+}$ animals was used as the negative and positive controls for $p19^{ARF}$, respectively. (E) Frozen sections of adipose tissue of $HuR^{fl/fl}$ and $HuR^{fl/fl}$; AP2-CRE mice (9 months old) were immunostained using $p19^{ARF}$ and HuR antibodies. Sections were counterstained with DAPI. Bars, 20 μm. (F) Rates of $p19^{ARF}$-positive cells in panel E were plotted. WAT, white adipose tissue. (G) *PAI-1* mRNA levels were analyzed using real-time PCR.

$p16^{Ink4a}$-Rb pathway plays pivotal roles in cell cycle arrest during cellular senescence in human cells. In contrast, it has been well established that the $p19^{ARF}$-p53 pathway is essential and that $p16^{Ink4a}$ is dispensable in the senescence of mouse cells. Consistently with these concepts, our results show that loss of HuR leads to increased expression of $p19^{ARF}$, but not $p16^{Ink4a}$, levels in MEFs. We further demonstrated that senescence caused by HuR loss can be abrogated by either *ARF* or *p53* deletion. Therefore, under normal conditions in which cells express sufficient amounts of HuR protein, $p19^{ARF}$ expression is suppressed, thereby protecting cells from undergoing p53-dependent replicative senescence. Additionally, it has been proposed that HuR positively regulates the expression of Mdm2, which is a major E3 ligase for p53 protein, and is negatively regulated by $p19^{ARF}$ (50). Thus, HuR suppresses p53 activity by modulating the expression of multiple targets integrated into the p53 pathway. Although we do not formally ex-

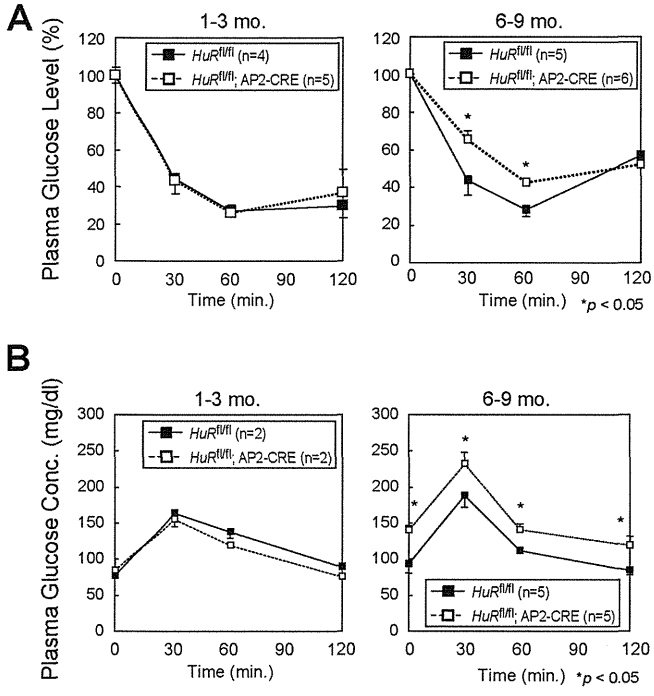

FIG 13 Adipose-specific HuR deletion accelerates age-dependent insulin resistance. Insulin tolerance tests (A) and glucose tolerance tests (B) were performed with $HuR^{fl/fl}$ and $HuR^{fl/fl}$; AP2-CRE mice.

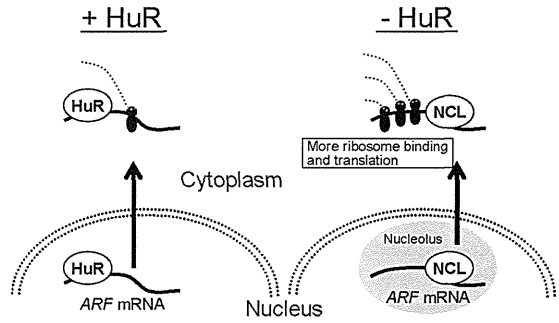

FIG 14 Model for *ARF* regulation by HuR and nucleolin. In the presence of HuR, *ARF* mRNA binds to HuR through the 5′UTR, and the mRNA localizes mainly to the nucleoplasm. The HuR-bound *ARF* mRNA is less efficiently translated. In the absence of HuR, *ARF* mRNA localizes to the nucleolus, where it associates with nucleolin (NCL). The nucleolin association facilitates ribosome binding, thereby enhancing the translation.

clude the possibility that $p16^{Ink4a}$ is also involved, it is conceivable that the $p19^{ARF}$-p53 pathway is a major target of HuR to control the life span of mouse cells.

In human cells, HuR directly associates with ARE in the 3′UTR of *Ink4a* mRNA (25). This region is shared by *ARF* mRNA; therefore, it is possible that HuR also regulates $p14^{ARF}$ expression in human cells. Unlike in human cells, in MEFs, the loss of HuR has no influence on $p16^{Ink4a}$ levels, while $p19^{ARF}$ is increased. Consistently with these results, HuR associates with the 5′UTR of *ARF* mRNA, which is not shared by *Ink4a*. However, the interaction of HuR with *ARF* mRNA is weak and observed only after UV-mediated cross-linking. Therefore, it is likely that HuR forms a much more fragile complex with *ARF* mRNA than with other mRNAs. Alternatively, the effect of HuR may be indirect; HuR may target another factor(s) that regulates $p19^{ARF}$ expression. In this regard, it is worthy of note that HuR regulates the translation of β-*catenin* and *Jun-B* mRNAs by modifying the stability of linc-p21 RNA (51). This could be clarified by identifying *ARF* mRNA-interacting molecules. Additionally, HuR has been proposed to recruit RISC to human *Ink4a* mRNA independently of miRNA, thereby destabilizing it (25). Although the involvement of miRNA needs to be further clarified, it is possible that RISC-mediated regulation may also be involved in mice, since deletion of *dicer-1* causes $p19^{ARF}$-p53-dependent cellular senescence (52). Furthermore, we detected *ARF* mRNA in the Ago2 complex. Nonetheless, the interaction of Ago2 and *ARF* mRNA was not decreased upon HuR depletion, implying that RISC is not involved in HuR-mediated *ARF* regulation.

HuR exclusively affects translation in $p19^{ARF}$ expression. Loss of HuR enhances ribosome association with *ARF* mRNA. This translational activation is associated with the nucleolar accumulation of *ARF* mRNA. We found that *ARF* mRNA associates with nucleolin, which is required for $p19^{ARF}$ induction in HuR-depleted cells. Nucleolin associates with numerous mRNAs and shuttles between the nucleolus and the cytoplasm. The influences of nucleolin on target mRNA differ depending on the target transcript. A recent report by Abdelmohsen and colleagues demonstrated that nucleolin is required for ribosome binding and subsequent translation of its target mRNA (45). Consistently with our results, they also observed *CDKN2A*, as well as both *ARF* and *Ink4a*, among the nucleolin-associated mRNAs. Together with these observations, our data suggest that HuR-associated *ARF* mRNA is retained in the nucleoplasm and is not efficiently translated upon nuclear export (Fig. 14). However, in the absence of HuR, *ARF* mRNA localizes to the nucleolus, where it associates with nucleolin. As nucleolin enhances ribosome recruitment to its target mRNA (45), $p19^{ARF}$ synthesis is increased under these conditions. Interestingly, *p53* mRNA also accumulates in the nucleoli upon DNA damage, when *p53* mRNA translation is increased (44). Hence, nucleolar localization of mRNA may reflect general aspects of stress-dependent mRNA translation. It has recently been shown by Miceli and colleagues that oncogenic Ras activates the transcription of the *ARF* gene, as well as the translation of *ARF* mRNA through mTORC1 (53). In this context, it is noteworthy that mTORC1 activity can affect the binding of HuR to *ornithine decarboxylase* mRNA (54). Therefore, it would be interesting to see if mTORC1 and HuR cooperate in *ARF* mRNA regulation.

Cellular senescence is known to be involved in metabolic disorders as well as cancers. Among these, senescence in adipose tissue is associated with insulin resistance (46). HuR has also been shown to function in adipocytes by regulating C/EBPβ expression (55, 56). Our results reveal that, although C/EBPβ may be affected by HuR status, it has little effect on adipogenesis, which is consistent with a previous report that *C/EBPβ*-null MEFs are capable of undergoing adipogenesis (57). Instead, the function of HuR in adipogenesis depends largely on *ARF*, as HuR knockdown had virtually no effect on adipogenesis in *ARF*-null MEF or 3T3-L1 cells, in which the p53 pathway was inactivated by *mdm2* amplification (Fig. 11 and data not shown) (58). Impaired adipogenesis is observed with concomitant reductions in clonal expansion during the initial stage of adipogenesis, which is alleviated in an *ARF*-null background. Hence, it is likely that adipogenic failure in HuR-depleted MEFs is attributed largely to $p19^{ARF}$. There were no ab-

normalities in the shapes and sizes of adipose tissues in adipose-specific *HuR* knockout mice. However, these mice revealed progressive insulin resistance with age. The reason why this phenotype was not observed in young animals can be explained by differences in the levels of *ARF* mRNA among these animals. In young mice, increased translation by HuR loss does not lead to expression of sufficient amounts of p19^{ARF} because of low *ARF* mRNA levels. However, in older animals, larger amounts of *ARF* mRNA and an increased rate of translation synergistically induced p19^{ARF} in adipose tissue. SA-β-Gal activity was not as strong as in cultured cells, and we failed to quantitatively detect an increase in enzyme activity. Nonetheless, the senescence program is likely activated in those cells, since *PAI-1* was significantly induced. It should be further clarified whether the phenotype is completely dependent on p19^{ARF} or whether other adipocyte-related factors are involved. Also, it would be interesting to see if HuR is linked to metabolic disorders, such as type 2 diabetes mellitus. In this regard, it is noteworthy that there was strong linkage between the human *ARF* and *Ink4a* loci and the disease (59–61).

HuR is deregulated in many types of cancers (40), and there is no doubt that cellular senescence is a central tumor-suppressive mechanism in mammals. Hence, it is plausible that deregulated HuR activity and expression leads to an uncontrolled senescence program, thereby allowing cells to bypass senescence. This can be achieved by suppressing the activity of the p16^{Ink4a}-Rb pathway and the p19^{ARF}-p53 pathway in humans and mice, respectively. Moreover, HuR is downregulated in aged human tissues, which may contribute to an age-associated phenotype, such as decreased insulin sensitivity. Our data demonstrate a novel function of HuR in the maintenance of the cellular replicative life span and will lead to further understanding of the mechanism and biological roles of cellular senescence.

ACKNOWLEDGMENTS

We thank Leo Tsuda for providing the GFP-L10 construct, Takashi Funatsu for providing MS2-EGFP-NLS cDNA, and Noboru Motoyama for his valuable discussion and technical support.

This work was supported by grants from the Japanese Ministry of Education, Culture, Science, and Technology (grant 22790879) and the Japan Health Foundation.

We declare that we have no conflict of interest.

REFERENCES

1. **Hayflick L, Moorhead PS.** 1961. The serial cultivation of human diploid cell strains. Exp. Cell Res. **25**:585–621.
2. **Dimri GP, Lee X, Basile G, Acosta M, Scott G, Roskelley C, Medrano EE, Linskens M, Rubelj I, Pereira-Smith O, Peacocke M, Campisi J.** 1995. A biomarker that identifies senescent human cells in culture and in aging skin in vivo. Proc. Natl. Acad. Sci. U. S. A. **92**:9363–9367.
3. **Freund A, Orjalo AV, Desprez PY, Campisi J.** 2010. Inflammatory networks during cellular senescence: causes and consequences. Trends Mol. Med. **16**:238–246.
4. **Ben-Porath I, Weinberg RA.** 2005. The signals and pathways activating cellular senescence. Int. J. Biochem. Cell Biol. **37**:961–976.
5. **Sherr CJ.** 2006. Divorcing ARF and p53: an unsettled case. Nat. Rev. Cancer **6**:663–673.
6. **Campisi Jand D, d'Adda F.** 2007. Cellular senescence: when bad things happen to good cells. Nat. Rev. Mol. Cell Biol. **8**:729–740.
7. **Collado M, Blasco MA, Serrano M.** 2007. Cellular senescence in cancer and aging. Cell **130**:223–233.
8. **Good PJ.** 1995. A conserved family of elav-like genes in vertebrates. Proc. Natl. Acad. Sci. U. S. A. **92**:4557–4561.
9. **Ma WJ, Cheng S, Campbell C, Wright A, Furneaux H.** 1996. Cloning and characterization of HuR, a ubiquitously expressed Elav-like protein. J. Biol. Chem. **271**:8144–8151.
10. **Katsanou V, Milatos S, Yiakouvaki A, Sgantzis N, Kotsoni A, Alexiou M, Harokopos V, Aidinis V, Hemberger M, Kontoyiannis DL.** 2009. The RNA-binding protein Elavl1/HuR is essential for placental branching morphogenesis and embryonic development. Mol. Cell. Biol. **29**:2762–2776.
11. **Brennan CM, Steitz JA.** 2001. HuR and mRNA stability. Cell. Mol. Life Sci. **58**:266–277.
12. **Doller A, Pfeilschifter J, Eberhardt W.** 2008. Signalling pathways regulating nucleo-cytoplasmic shuttling of the mRNA-binding protein HuR. Cell. Signal. **20**:2165–2173.
13. **Abdelmohsen K, Lal A, Kim HH, Gorospe M.** 2007. Posttranscriptional orchestration of an anti-apoptotic program by HuR. Cell Cycle **6**:1288–1292.
14. **Hinman MN, Lou H.** 2008. Diverse molecular functions of Hu proteins. Cell. Mol. Life Sci. **65**:3168–3181.
15. **Dean JL, Wait R, Mahtani KR, Sully G, Clark AR, Saklatvala J.** 2001. The 3′ untranslated region of tumor necrosis factor alpha mRNA is a target of the mRNA-stabilizing factor HuR. Mol. Cell. Biol. **21**:721–730.
16. **Dormoy-Raclet V, Menard I, Clair E, Kurban G, Mazroui R, Di Marco S, von Roretz C, Pause A, Gallouzi IE.** 2007. The RNA-binding protein HuR promotes cell migration and cell invasion by stabilizing the beta-actin mRNA in a U-rich-element-dependent manner. Mol. Cell. Biol. **27**:5365–5380.
17. **Levy NS, Chung S, Furneaux H, Levy AP.** 1998. Hypoxic stabilization of vascular endothelial growth factor mRNA by the RNA-binding protein HuR. J. Biol. Chem. **273**:6417–6423.
18. **Lopez de Silanes I, Gorospe M, Taniguchi H, Abdelmohsen K, Srikantan S, Alaminos M, Berdasco M, Urdinguio RG, Fraga MF, Jacinto FV, Esteller M.** 2009. The RNA-binding protein HuR regulates DNA methylation through stabilization of DNMT3b mRNA. Nucleic Acids Res. **37**:2658–2671.
19. **Lal A, Mazan-Mamczarz K, Kawai T, Yang X, Martindale JL, Gorospe M.** 2004. Concurrent versus individual binding of HuR and AUF1 to common labile target mRNAs. EMBO J. **23**:3092–3102.
20. **Kim HH, Kuwano Y, Srikantan S, Lee EK, Martindale JL, Gorospe M.** 2009. HuR recruits let-7/RISC to repress c-Myc expression. Genes Dev. **23**:1743–1748.
21. **Tominaga K, Srikantan S, Lee EK, Subaran SS, Martindale JL, Abdelmohsen K, Gorospe M.** 2011. Competitive regulation of nucleolin expression by HuR and miR-494. Mol. Cell. Biol. **31**:4219–4231.
22. **Wang W, Yang X, Cristofalo VJ, Holbrook NJ, Gorospe M.** 2001. Loss of HuR is linked to reduced expression of proliferative genes during replicative senescence. Mol. Cell. Biol. **21**:5889–5898.
23. **Abdelmohsen K, Srikantan S, Kuwano Y, Gorospe M.** 2008. miR-519 reduces cell proliferation by lowering RNA-binding protein HuR levels. Proc. Natl. Acad. Sci. U. S. A. **105**:20297–20302.
24. **Marasa BS, Srikantan S, Martindale JL, Kim MM, Lee EK, Gorospe M, Abdelmohsen K.** 2010. MicroRNA profiling in human diploid fibroblasts uncovers miR-519 role in replicative senescence. Aging (Albany, NY) **2**:333–343.
25. **Chang N, Yi J, Guo G, Liu X, Shang Y, Tong T, Cui Q, Zhan M, Gorospe M, Wang W.** 2010. HuR uses AUF1 as a cofactor to promote p16INK4 mRNA decay. Mol. Cell. Biol. **30**:3875–3886.
26. **Mazan-Mamczarz K, Galban S, Lopez de Silanes I, Martindale JL, Atasoy U, Keene JD, Gorospe M.** 2003. RNA-binding protein HuR enhances p53 translation in response to ultraviolet light irradiation. Proc. Natl. Acad. Sci. U. S. A. **100**:8354–8359.
27. **Wang W, Furneaux H, Cheng H, Caldwell MC, Hutter D, Liu Y, Holbrook N, Gorospe M.** 2000. HuR regulates p21 mRNA stabilization by UV light. Mol. Cell. Biol. **20**:760–769.
28. **Krimpenfort P, Quon KC, Mooi WJ, Loonstra A, Berns A.** 2001. Loss of p16Ink4a confers susceptibility to metastatic melanoma in mice. Nature **413**:83–86.
29. **Sharpless NE, Bardeesy N, Lee KH, Carrasco D, Castrillon DH, Aguirre AJ, Wu EA, Horner JW, DePinho RA.** 2001. Loss of p16Ink4a with retention of p19Arf predisposes mice to tumorigenesis. Nature **413**:86–91.
30. **Yamagishi M, Ishihama Y, Shirasaki Y, Kurama H, Funatsu T.** 2009. Single-molecule imaging of beta-actin mRNAs in the cytoplasm of a living cell. Exp. Cell Res. **315**:1142–1147.
31. **Zindy F, Eischen CM, Randle DH, Kamijo T, Cleveland JL, Sherr CJ, Roussel MF.** 1998. Myc signaling via the ARF tumor suppressor regulates

p53-dependent apoptosis and immortalization. Genes Dev. 12:2424–2433.
32. Heiman M, Schaefer A, Gong S, Peterson JD, Day M, Ramsey KE, Suarez-Farinas M, Schwarz C, Stephan DA, Surmeier DJ, Greengard P, Heintz N. 2008. A translational profiling approach for the molecular characterization of CNS cell types. Cell 135:738–748.
33. Nakamura H, Kawagishi H, Watanabe A, Sugimoto K, Maruyama M, Sugimoto M. 2011. Cooperative role of the RNA-binding proteins Hzf and HuR in p53 activation. Mol. Cell. Biol. 31:1997–2009.
34. Todaro GJ, Green H. 1963. Quantitative studies of the growth of mouse embryo cells in culture and their development into established lines. J. Cell Biol. 17:299–313.
35. Mu XC, Higgins PJ. 1995. Differential growth state-dependent regulation of plasminogen activator inhibitor type-1 expression in senescent IMR-90 human diploid fibroblasts. J. Cell. Physiol. 165:647–657.
36. Harvey M, Sands AT, Weiss RS, Hegi ME, Wiseman RW, Pantazis P, Giovanella BC, Tainsky MA, Bradley A, Donehower LA. 1993. In vitro growth characteristics of embryo fibroblasts isolated from p53-deficient mice. Oncogene 8:2457–2467.
37. Palmero I, Pantoja C, Serrano M. 1998. p19ARF links the tumour suppressor p53 to Ras. Nature 395:125–126.
38. Serrano M, Lin AW, McCurrach ME, Beach D, Lowe SW. 1997. Oncogenic ras provokes premature cell senescence associated with accumulation of p53 and p16INK4a. Cell 88:593–602.
39. Tsukada T, Tomooka Y, Takai S, Ueda Y, Nishikawa S, Yagi T, Tokunaga T, Takeda N, Suda Y, Abe S. 1993. Enhanced proliferative potential in culture of cells from p53-deficient mice. Oncogene 8:3313–3322.
40. Abdelmohsen K, Gorospe M. 2010. Posttranscriptional regulation of cancer traits by HuR. Wiley Interdiscip. Rev. RNA 1:214–229.
41. Sherr CJ. 2001. The INK4a/ARF network in tumour suppression. Nat. Rev. Mol. Cell Biol. 2:731–737.
42. Doyle JP, Dougherty JD, Heiman M, Schmidt EF, Stevens TR, Ma G, Bupp S, Shrestha P, Shah RD, Doughty ML, Gong S, Greengard P, Heintz N. 2008. Application of a translational profiling approach for the comparative analysis of CNS cell types. Cell 135:749–762.
43. Fusco D, Accornero N, Lavoie B, Shenoy SM, Blanchard JM, Singer RH, Bertrand E. 2003. Single mRNA molecules demonstrate probabilistic movement in living mammalian cells. Curr. Biol. 13:161–167.
44. Gajjar M, Candeias MM, Malbert-Colas L, Mazars A, Fujita J, Olivares-Illana V, Fahraeus R. 2012. The p53 mRNA-Mdm2 interaction controls Mdm2 nuclear trafficking and is required for p53 activation following DNA damage. Cancer Cell 21:25–35.
45. Abdelmohsen K, Tominaga K, Lee EK, Srikantan S, Kang MJ, Kim MM, Selimyan R, Martindale JL, Yang X, Carrier F, Zhan M, Becker KG, Gorospe M. 2011. Enhanced translation by Nucleolin via G-rich elements in coding and non-coding regions of target mRNAs. Nucleic Acids Res. 39:8513–8530.
46. Minamino T, Orimo M, Shimizu I, Kunieda T, Yokoyama M, Ito T, Nojima A, Nabetani A, Oike Y, Matsubara H, Ishikawa F, Komuro I. 2009. A crucial role for adipose tissue p53 in the regulation of insulin resistance. Nat. Med. 15:1082–1087.
47. Cherry J, Jones H, Karschner VA, Pekala PH. 2008. Post-transcriptional control of CCAAT/enhancer-binding protein beta (C/EBPbeta) expression: formation of a nuclear HuR-C/EBPbeta mRNA complex determines the amount of message reaching the cytosol. J. Biol. Chem. 283:30812–30820.
48. Krishnamurthy J, Torrice C, Ramsey MR, Kovalev GI, Al Regaiey K, Su L, Sharpless NE. 2004. Ink4a/Arf expression is a biomarker of aging. J. Clin. Invest. 114:1299–1307.
49. Kamijo T, Zindy F, Roussel MF, Quelle DE, Downing JR, Ashmun RA, Grosveld G, Sherr CJ. 1997. Tumor suppression at the mouse INK4a locus mediated by the alternative reading frame product p19ARF. Cell 91:649–659.
50. Ghosh M, Aguila HL, Michaud J, Ai Y, Wu MT, Hemmes A, Ristimaki A, Guo C, Furneaux H, Hla T. 2009. Essential role of the RNA-binding protein HuR in progenitor cell survival in mice. J. Clin. Invest. 119:3530–3543.
51. Yoon JH, Abdelmohsen K, Srikantan S, Yang X, Martindale JL, De S, Huarte M, Zhan M, Becker KG, Gorospe M. 2012. lincRNA-p21 suppresses target mRNA translation. Mol. Cell 47:648–655.
52. Mudhasani R, Zhu Z, Hutvagner G, Eischen CM, Lyle S, Hall LL, Lawrence JB, Imbalzano AN, Jones SN. 2008. Loss of miRNA biogenesis induces p19Arf-p53 signaling and senescence in primary cells. J. Cell Biol. 181:1055–1063.
53. Miceli AP, Saporita AJ, Weber JD. 2012. Hypergrowth mTORC1 signals translationally activate the ARF tumor suppressor checkpoint. Mol. Cell. Biol. 32:348–364.
54. Origanti S, Nowotarski SL, Carr TD, Sass-Kuhn S, Xiao L, Wang JY, Shantz LM. 2012. Ornithine decarboxylase mRNA is stabilized in an mTORC1-dependent manner in Ras-transformed cells. Biochem. J. 442:199–207.
55. Gantt K, Cherry J, Tenney R, Karschner V, Pekala PH. 2005. An early event in adipogenesis, the nuclear selection of the CCAAT enhancer-binding protein β (C/EBPβ) mRNA by HuR and its translocation to the cytosol. J. Biol. Chem. 280:24768–24774.
56. Jones H, Carver M, Pekala PH. 2007. HuR binds to a single site on the C/EBPbeta mRNA of 3T3-L1 adipocytes. Biochem. Biophys. Res. Commun. 355:217–220.
57. Tanaka T, Yoshida N, Kishimoto T, Akira S. 1997. Defective adipocyte differentiation in mice lacking the C/EBPbeta and/or C/EBPdelta gene. EMBO J. 16:7432–7443.
58. Berberich SJ, Litteral V, Mayo LD, Tabesh D, Morris D. 1999. mdm-2 gene amplification in 3T3-L1 preadipocytes. Differentiation 64:205–212.
59. Saxena R, Voight BF, Lyssenko V, Burtt NP, de Bakker PI, Chen H, Roix JJ, Kathiresan S, Hirschhorn JN, Daly MJ, Hughes TE, Groop L, Altshuler D, Almgren P, Florez JC, Meyer J, Ardlie K, Bengtsson K, Isomaa B, Lettre G, Lindblad U, Lyon HN, Melander O, Newton-Cheh C, Nilsson P, Orho-Melander M, Rastam L, Speliotes EK, Taskinen MR, Tuomi T, Guiducci C, Berglund A, Carlson J, Gianniny L, Hackett R, Hall L, Holmkvist J, Laurila E, Sjogren M, Sterner M, Surti A, Svensson M, Svensson M, Tewhey R, Blumenstiel B, Parkin M, Defelice M, Barry R, Brodeur W, Camarata J, Chia N, Fava M, Gibbons J, Handsaker B, Healy C, Nguyen K, Gates C, Sougnez C, Gage D, Nizzari M, Gabriel SB, Chirn GW, Ma Q, Parikh H, Richardson D, Ricke D, Purcell S. 2007. Genome-wide association analysis identifies loci for type 2 diabetes and triglyceride levels. Science 316:1331–1336.
60. Scott LJ, Mohlke KL, Bonnycastle LL, Willer CJ, Li Y, Duren WL, Erdos MR, Stringham HM, Chines PS, Jackson AU, Prokunina-Olsson L, Ding CJ, Swift AJ, Narisu N, Hu T, Pruim R, Xiao R, Li XY, Conneely KN, Riebow NL, Sprau AG, Tong M, White PP, Hetrick KN, Barnhart MW, Bark CW, Goldstein JL, Watkins L, Xiang F, Saramies J, Buchanan TA, Watanabe RM, Valle TT, Kinnunen L, Abecasis GR, Pugh EW, Doheny KF, Bergman RN, Tuomilehto J, Collins FS, Boehnke M. 2007. A genome-wide association study of type 2 diabetes in Finns detects multiple susceptibility variants. Science 316:1341–1345.
61. Zeggini E, Weedon MN, Lindgren CM, Frayling TM, Elliott KS, Lango H, Timpson NJ, Perry JR, Rayner NW, Freathy RM, Barrett JC, Shields B, Morris AP, Ellard S, Groves CJ, Harries LW, Marchini JL, Owen KR, Knight B, Cardon LR, Walker M, Hitman GA, Morris AD, Doney AS, McCarthy MI, Hattersley AT. 2007. Replication of genome-wide association signals in U.K. samples reveals risk loci for type 2 diabetes. Science 316:1336–1341.

Brief report

Somatic mosaicism for oncogenic *NRAS* mutations in juvenile myelomonocytic leukemia

Sayoko Doisaki,[1] Hideki Muramatsu,[1] Akira Shimada,[1] Yoshiyuki Takahashi,[1] Makiko Mori-Ezaki,[2] Masanori Sato,[3] Hiroyuki Kawaguchi,[4] Akitoshi Kinoshita,[5] Manabu Sotomatsu,[6] Yasuhide Hayashi,[6] Yoko Furukawa-Hibi,[7] Kiyofumi Yamada,[7] Hideaki Hoshino,[8] Hitoshi Kiyoi,[8] Nao Yoshida,[9] Hirotoshi Sakaguchi,[1] Atsushi Narita,[1] Xinan Wang,[1] Olfat Ismael,[1] Yinyan Xu,[1] Nobuhiro Nishio,[1] Makito Tanaka,[1] Asahito Hama,[1] Kenichi Koike,[10] and Seiji Kojima[1]

[1]Department of Pediatrics, Nagoya University Graduate School of Medicine, Nagoya, Japan; [2]Department of Hematology Oncology, Saitama Children's Medical Center, Saitama, Japan; [3]Department of Pediatrics, Tokyo Dental College Ichikawa General Hospital, Ichikawa, Japan; [4]Department of Pediatrics, National Defense Medical College, Tokorozawa, Japan; [5]Department of Pediatrics, St Marianna University School of Medicine, Kawasaki, Japan; [6]Department of Hematology/Oncology, Gunma Children's Medical Center, Shibukawa, Japan; [7]Department of Neuropsychopharmacology and Hospital Pharmacy, Nagoya University Graduate School of Medicine, Nagoya, Japan; [8]Department of Hematology and Oncology, Nagoya University Graduate School of Medicine, Nagoya, Japan; [9]Department of Pediatrics, Japanese Red Cross Nagoya First Hospital, Nagoya, Japan; and [10]Department of Pediatrics, Shinshu University School of Medicine, Matsumoto, Japan

Juvenile myelomonocytic leukemia (JMML) is a rare pediatric myeloid neoplasm characterized by excessive proliferation of myelomonocytic cells. Somatic mutations in genes involved in GM-CSF signal transduction, such as *NRAS*, *KRAS*, *PTPN11*, *NF1*, and *CBL*, have been identified in more than 70% of children with JMML. In the present study, we report 2 patients with somatic mosaicism for oncogenic *NRAS* mutations (G12D and G12S) associated with the development of JMML. The mutated allele frequencies quantified by pyrosequencing were various and ranged from 3%-50% in BM and other somatic cells (ie, buccal smear cells, hair bulbs, or nails). Both patients experienced spontaneous improvement of clinical symptoms and leukocytosis due to JMML without hematopoietic stem cell transplantation. These patients are the first reported to have somatic mosaicism for oncogenic *NRAS* mutations. The clinical course of these patients suggests that *NRAS* mosaicism may be associated with a mild disease phenotype in JMML. (*Blood*. 2012;120(7):1485-1488)

Introduction

Juvenile myelomonocytic leukemia (JMML) is a rare myeloid neoplasm characterized by excessive proliferation of myelomonocytic cells. Somatic mutations in genes involved in GM-CSF signal transduction, such as *NRAS*, *KRAS*, *PTPN11*, *NF1*, and *CBL*, have been identified in more than 70% of children with JMML.[1-3] The term "somatic mosaicism" is defined as the presence of multiple populations of cells with distinct genotypes in one person whose developmental lineages trace back to a single fertilized egg.[4] Somatic mosaicism of various genes, including some oncogenes, has been implicated in many diseases. For example, somatic mosaicism for *HRAS* mutations is found in patients with Costello syndrome.[5-7] Whereas germline mutations in causative genes (ie, *PTPN11*, *NRAS*, *NF1*, and *CBL*) are found in JMML patients,[3,8-11] the presence of somatic mosaicism for these genes has never been reported. In the present study, we describe 2 cases of JMML in which the patients display somatic mosaicism for oncogenic *NRAS* mutations (G12D and G12S).

Study design

Written informed consent for sample collection was obtained from the patients' parents in accordance with the Declaration of Helsinki, and molecular analysis of the mutational status was approved by the ethics committee of the Nagoya University Graduate School of Medicine (Nagoya, Japan).

Patient 1. A 10-month-old boy had hepatosplenomegaly and leukocytosis (72.1×10^9/L) with monocytosis (13.3×10^9/L; Table 1). The patient's BM contained 7% blasts with myeloid hyperplasia. Cytogenetic analysis revealed a normal karyotype and colony assay of BM mononuclear cells (BM-MNCs) showed spontaneous colony formation but GM-CSF hypersensitivity assay was not tested. The diagnostic criteria for JMML, as developed by the European Working Group on Myelodysplastic Syndrome in Childhood, was fulfilled,[12] and the patient was treated with IFN-α and 6-mercaptopurine. His clinical and laboratory findings gradually resolved without hematopoietic stem cell transplantation. However, 11 years after the diagnosis of JMML, the patient developed thrombocytopenia (7.6×10^9/L) and BM findings showed trilineage dysplasia with low blast count compatible with refractory anemia. The patient did not have any physiologic abnormalities, such as facial deformity, and there was no family history of malignancy or congenital abnormalities.

Patient 2. A 10-month-old boy had anemia, hepatosplenomegaly, and leukocytosis (31.8×10^9/L) with monocytosis (6.4×10^9/L; Table 1). The patient's BM exhibited myeloid hyperplasia and granulocytic dysplasia with 5% blasts. Cytogenetic

Submitted February 3, 2012; accepted June 11, 2012. Prepublished online as *Blood* First Edition paper, July 2, 2012; DOI 10.1182/blood-2012-02-406090.

The online version of this article contains a data supplement.

The publication costs of this article were defrayed in part by page charge payment. Therefore, and solely to indicate this fact, this article is hereby marked "advertisement" in accordance with 18 USC section 1734.

Table 1. Patient characteristics

	Patient 1	Patient 2
Age, mo	10	10
Sex	Male	Male
Liver, cm	12	5
Spleen, cm	8	10
WBCs, $\times 10^9$/L	72.1	31.8
Monocytes, %	18.5	20
Blasts, %	4	2
Hb, g/dL	8.9	5.4
Platelets, $\times 10^9$/L	59	100
HbF, %	2.1	1.7
BM blasts, %	7	5
Karyotype	46,XY [20/20]	46,XY [20/20]
Monosomy 7 (FISH)	Negative	Negative
Spontaneous colony formation	Positive	Positive
Gene mutation	*NRAS*, G12D 35G > A	*NRAS*, G12S 34G > A
Treatment	IFN-α-2b, 6-MP	None
Observation period, mo	231	103
Outcome	Alive	Alive
Fraction of mutant alleles, % (pyrosequencing)		
Nail (whole)	24	12.5 (average)
Nail (left hand)	ND	26
Nail (right hand)	ND	13
Nail (left foot)	ND	8
Nail (right foot)	ND	3
Buccal smear cells	43	21
Hair bulbs	5	ND
Family studies		
Father	Wild-type	Wild-type
Mother	Wild-type	Wild-type
Sibling	ND	Wild-type

Hb indicates hemoglobin; 6-MP, 6-mercaptopurine; and ND, not done.

analysis revealed a normal karyotype. Colony assay of BM-MNCs showed spontaneous colony formation and GM-CSF hypersensitivity. Although the diagnostic criteria for JMML were fulfilled,[12] the patient's clinical symptoms and leukocytosis improved spontaneously within a few months without cytotoxic therapy or hematopoietic stem cell transplantation. The patient has remained healthy and has experienced no hematologic or physiologic abnormalities. The most recent follow-up examination was conducted when the patient was 8 years of age.

Detailed methods for experiments are described in supplemental Methods (available on the *Blood* Web site; see the Supplemental Materials link at the top of the online article).

Results and discussion

DNA sequencing for JMML-associated genes (ie, *NRAS*, *KRAS*, *PTPN11*, and *CBL*) was performed (Figure 1 and Table 1). In Patient 1, the *NRAS* G12D mutation was identified in BM-MNCs at the time of diagnosis of both JMML and MDS. We identified the same G12D mutation in DNA derived from buccal smear cells and nails of both hands; however, the sequence profile of the nails showed a low signal for the mutant allele compared with signal of blood cells. In Patient 2, the *NRAS* G12S mutation was identified in DNA from BM-MNCs, buccal smear cells, and nails of the left hand. However, the sequence profiles of buccal smear cells and nails of the left hand showed a low signal for the mutant variant. No mutation was detected in DNA from the PB-MNCs of the patient's parents or sibling.

We used pyrosequencing to quantify the fraction of mutated alleles in DNA samples from different somatic tissues (Figure 1 and Table 1). The frequency of mutated alleles varied by tissue type as follows. For Patient 1: BM-MNCs, 50%; nails, 24%; buccal smear cells, 43%; and hair bulbs, 5%. For Patient 2: buccal smear cells, 21%; nails of left hand, 26%; nails of right hand, 13%; nails of left foot, 8%; and nails of right foot, 3%. We cloned the PCR product of *NRAS* exon 2 from the nails of Patient 1 and picked up 15 clones. The clones were sequenced. Four of the 15 clones (27%) contained the mutant allele, which is consistent with the results of pyrosequencing analysis (24% mutant allele). Because the confirmed detection level by pyrosequencing technique was above 5%, results with a low percentage (< 5%) of mutant allele (ie, hair bulbs in Patient 1) should be interpreted with caution.[13,14]

We diagnosed 2 JMML patients as having somatic mosaicism of *NRAS* mutations: G12D for Patient 1 and G12S for Patient 2. The diagnoses were based on negative familial studies and mutational allele quantification analyses that showed diversity in the chimeric mutational status of different somatic tissues. Although DNA from buccal smear cells might be contaminated with WBCs, we also identified mutations in DNA from the nail tissue, which is known to be a good biologic material without contamination from hematopoietic cells, in both patients. These data suggest that a portion of the *NRAS*-mutated somatic cells were derived from one cell that acquired the mutation at a very early developmental stage. Although both somatic and germline mutations of RAS pathway genes (ie, *PTPN11*, *NRAS*, *NF1*, and *CBL*) are found in some JMML patients,[3,8-11] somatic mosaicism for these genes has never been reported. To the best of our knowledge, the present study is

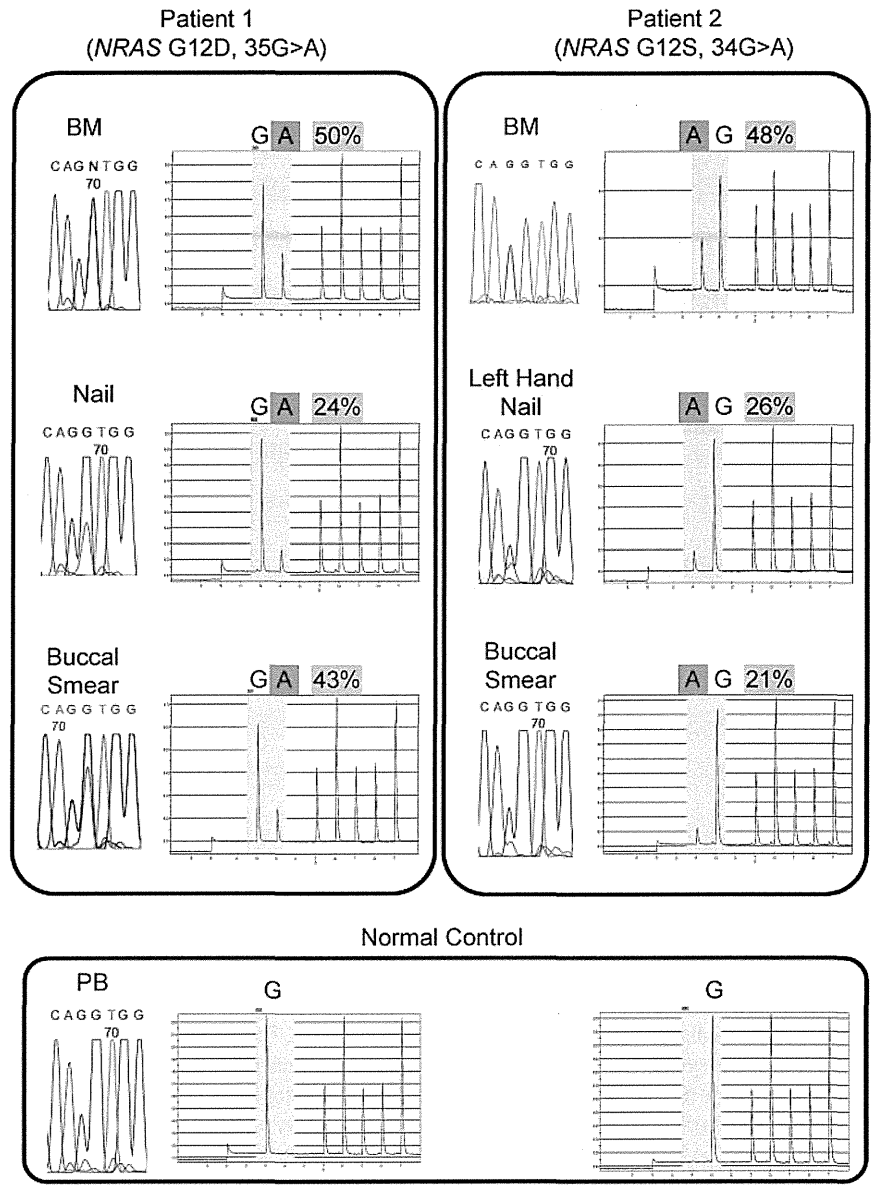

Figure 1. Direct sequencing and quantitative mutational analysis of *NRAS* in JMML patients. *NRAS* mutations are detected by direct sequencing and quantified by pyrosequencing. Direct sequencing identified oncogenic *NRAS* mutations: for Patient 1, G12D, 35G > A; for Patient 2, G12S, 34G > A) in BM-MNCs at diagnosis of JMML and in the nails and buccal smear cells. Quantification by pyrosequencing revealed that the fractions of mutated allele varied among different tissue types. For Patient 1: BM, 50%; nail, 24%; and buccal smear, 43%. For Patient 2: BM, 48%; left-hand nail, 26%; and buccal smear, 21%.

the first report of JMML patients with somatic mosaicism of mutations in RAS pathway genes.

Germline RAS pathway mutations are often associated with dysmorphic features similar to Noonan syndrome or its associated diseases. Correspondingly, JMML patients with germline *NRAS* or *CBL* mutations exhibit characteristic dysmorphic features.[3,10] Although our patients did not show any dysmorphic or developmental abnormalities, they should receive careful medical follow-up, especially for the occurrence of other cancers, because of the oncogenic nature of the mutations.

In general, JMML is a rapidly fatal disorder if left untreated.[8] However, recent clinical genotype-phenotype analyses have revealed heterogeneity in their clinical course. We and other researchers have reported that patients with *PTPN11* mutations have a worse prognosis than patients with other gene mutations, including *NRAS* and *KRAS*.[15,16] Both of the JMML patients in the present study with somatic mosaicism of oncogenic *NRAS* mutations have had a mild and self-limiting clinical course. We analyzed nails of other 3 JMML patients with RAS mutations who experienced aggressive clinical course and none showed somatic mosaicism (data not shown). In analogy to the mild phenotype of JMML patients with germline mutations in *PTPN11*, we speculate that JMML patients with somatic mosaicism of RAS genes might have a mild clinical course. We are planning to confirm these observations in larger cohort.

Acknowledgments

The authors thank Ms Yoshie Miura, Ms Yuko Imanishi, and Ms Hiroe Namizaki for their valuable assistance with sample preparation and clerical work.

Authorship

Contribution: S.D. and H.M. designed and conducted the research, analyzed the data, and wrote the manuscript; A.S., M.M.-E., M. Sato, H.K., A.K., M. Sotomatsu, and Y.H. treated the patients; Y.T., Y.F.-H., K.Y., H.H., H.K., N.Y., H.S., A.N., X.W., O.I., Y.X.,

N.N., M.T., A.H., and K.K. conducted the research; and S.K. designed the research, analyzed the data, and wrote the manuscript.

Conflict-of-interest disclosure: The authors declare no competing financial interests.

Correspondence: Seiji Kojima, Department of Pediatrics, Nagoya University Graduate School of Medicine, 65 Tsuruma-cho, Showa-ku, Nagoya 466-8550, Japan; e-mail: kojimas@med.nagoya-u.ac.jp.

References

1. Flotho C, Kratz CP, Niemeyer CM. How a rare pediatric neoplasia can give important insights into biological concepts: a perspective on juvenile myelomonocytic leukemia. *Haematologica.* 2007; 92(11):1441-1446.
2. Muramatsu H, Makishima H, Jankowska AM, et al. Mutations of an E3 ubiquitin ligase c-Cbl but not TET2 mutations are pathogenic in juvenile myelomonocytic leukemia. *Blood.* 2010;115(10): 1969-1975.
3. Niemeyer CM, Kang MW, Shin DH, et al. Germline CBL mutations cause developmental abnormalities and predispose to juvenile myelomonocytic leukemia. *Nat Genet.* 2010;42(9):794-800.
4. Cotterman CW. Somatic mosaicism for antigen A2. *Acta Genet Stat Med.* 1956;6(4):520-521.
5. Gripp KW, Stabley DL, Nicholson L, Hoffman JD, Sol-Church K. Somatic mosaicism for an HRAS mutation causes Costello syndrome. *Am J Med Genet A.* 2006;140(20):2163-2169.
6. Sol-Church K, Stabley DL, Demmer LA, et al. Male-to-male transmission of Costello syndrome: G12S HRAS germline mutation inherited from a father with somatic mosaicism. *Am J Med Genet A.* 2009;149A(3):315-321.
7. Girisha KM, Lewis LE, Phadke SR, Kutsche K. Costello syndrome with severe cutis laxa and mosaic HRAS G12S mutation. *Am J Med Genet A.* 2010;152A(11):2861-2864.
8. Niemeyer CM, Arico M, Basso G, et al. Chronic myelomonocytic leukemia in childhood: a retrospective analysis of 110 cases. European Working Group on Myelodysplastic Syndromes in Childhood (EWOG-MDS). *Blood.* 1997;89(10): 3534-3543.
9. Tartaglia M, Niemeyer CM, Fragale A, et al. Somatic mutations in PTPN11 in juvenile myelomonocytic leukemia, myelodysplastic syndromes and acute myeloid leukemia. *Nat Genet.* 2003; 34(2):148-150.
10. De Filippi P, Zecca M, Lisini D, et al. Germ-line mutation of the NRAS gene may be responsible for the development of juvenile myelomonocytic leukaemia. *Br J Haematol.* 2009;147(5):706-709.
11. Side LE, Emanuel PD, Taylor B, et al. Mutations of the NF1 gene in children with juvenile myelomonocytic leukemia without clinical evidence of neurofibromatosis, type 1. *Blood.* 1998;92(1): 267-272.
12. Pinkel D. Differentiating juvenile myelomonocytic leukemia from infectious disease [letter]. *Blood.* 1998;91(1):365-367.
13. Fakhrai-Rad H, Pourmand N, Ronaghi M. Pyrosequencing: an accurate detection platform for single nucleotide polymorphisms. *Hum Mutat.* 2002;19(5):479-485.
14. Ogino S, Kawasaki T, Brahmandam M, et al. Sensitive sequencing method for KRAS mutation detection by Pyrosequencing. *J Mol Diagn.* 2005; 7(3):413-421.
15. Bresolin S, Zecca M, Flotho C, et al. Gene expression-based classification as an independent predictor of clinical outcome in juvenile myelomonocytic leukemia. *J Clin Oncol.* 2010; 28(11):1919-1927.
16. Yoshida N, Yagasaki H, Xu Y, et al. Correlation of clinical features with the mutational status of GM-CSF signaling pathway-related genes in juvenile myelomonocytic leukemia. *Pediatr Res.* 2009;65(3):334-340.

Open

Leukemia (2012) **26,** 1879 – 1898

www.nature.com/leu

LETTERS TO THE EDITOR

Novel splicing-factor mutations in juvenile myelomonocytic leukemia

Leukemia (2012) **26,** 1879–1881; doi:10.1038/leu.2012.45

Myelodysplastic syndromes (MDS) and myelodysplastic/myeloproliferative neoplasms (MDS/MPN) are heterogeneous groups of chronic myeloid neoplasms characterized by clonal hematopoiesis, varying degrees of cytopenia or myeloproliferative features with evidence of myelodysplasia and a propensity to acute myeloid leukemia (AML).[1] In recent years, a number of novel gene mutations, involving *TET2*, *ASXL1*, *DNMT3A*, *EZH2*, *IDH1/2*, and *c-CBL*, have been identified in adult cases of chronic myeloid neoplasms, which have contributed to our understanding of disease pathogenesis.[2–7] However, these mutations are rare in pediatric cases, with the exception of germline or somatic *c-CBL* mutations found in 10–15% of chronic myelomonocytic leukemia (CMML) and juvenile myelomonocytic leukemia (JMML),[8] highlighting the distinct pathogenesis of adult and pediatric neoplasms.[9]

Recently, we reported high frequencies of mutations, involving the RNA splicing machinery, that are largely specific to myeloid neoplasms, showing evidence of myeloid dysplasia in adult.[10] Affecting a total of eight components of the RNA splicing machinery (U2AF35, U2AF65, SF3A1, SF3B1, SRSF2, ZRSR2, SF1 and PRPF40B) commonly involved in the 3′ splice-site (3′SS) recognition, these pathway mutations are now implicated in the pathogenesis of myelodysplasia.[10] To investigate the role of the splicing-pathway mutations in the pathogenesis of pediatric myeloid malignancies, we have examined 165 pediatric cases with AML, MDS, chronic myeloid leukemia (CML) and JMML for mutations in the four major splicing factors, *U2AF35*, *ZRSR2*, *SRSF2*, and *SF3B1*, commonly mutated in adult cases.

Bone marrow or peripheral blood tumor specimens were obtained from 165 pediatric patients with various myeloid malignancies, including *de novo* AML ($n=93$), MDS ($n=28$), CML ($n=17$) and JMML ($n=27$), and the genomic DNA (gDNA) was subjected to mutation analysis (Supplementary Table 1). The status of the RAS pathway mutations for the current JMML series has been reported previously (Supplementary Table 2).[11,12] Nineteen leukemia cell lines derived from AML (YNH-1, ML-1, KASUMI-3, KG-1, HL60, inv-3, SN-1, NB4 and HEL), acute monocytic leukemia (THP-1, SCC-3, J-111, CTS, P31/FUJ, MOLM-13, IMS/MI and KOCL-48) and acute megakaryoblastic leukemia (CMS and CMY) were also analyzed for mutations. Peripheral blood gDNA from 60 healthy adult volunteers was used as controls. Informed consent was obtained from the patients and/or their parents and from the healthy volunteers. We previously showed that for *U2AF35*, *SRSF2* and *SF3B1*, most of the mutations in adult cases were observed in exons 2 and 7, exon 1, and exons 14 and 15, respectively.[10] Therefore, we confirmed mutation screening to these 'hot-spot' exons. In contrast, all the coding exons were examined for *ZRSR2*, because no mutational hot spots have been detected. Briefly, the relevant exons were amplified using PCR and mutations were examined by Sanger sequencing, as previously described.[10] The Fisher's exact test was used to evaluate the statistical significance of frequencies of mutations for *U2AF35*, *SF3B1*, *ZRSR2* or *SRSF2* in adult cases and pediatric cases. This study was approved by the Ethics Committee of the University of Tokyo (Approval number 948-7).

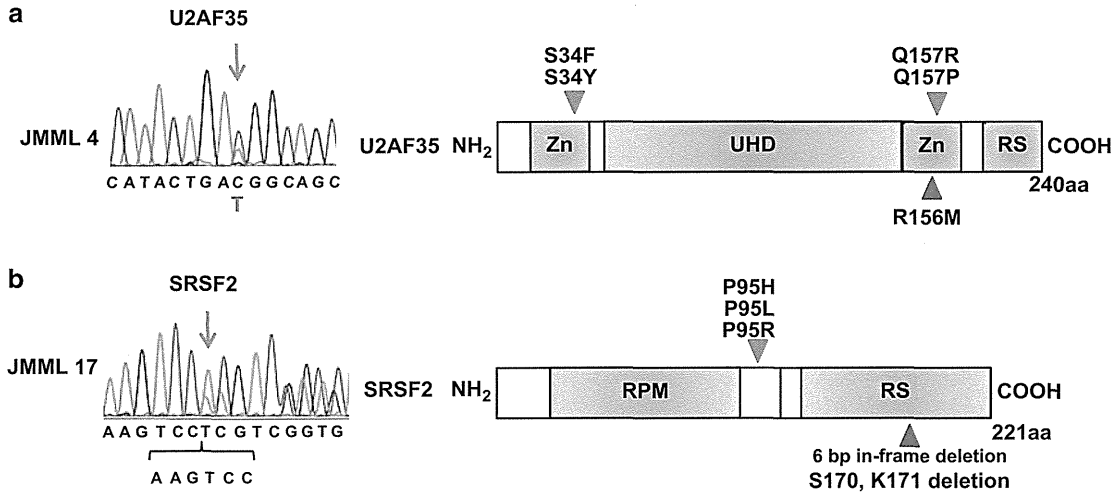

Figure 1. Novel *U2AF35*and *SRSF2* mutations detected in JMML cases. (**a**) Left panel: sequence chromatogram of a heterozygous mutation at R156 in N-terminal zinc-finger motifs of *U2AF35* detected in a JMML case (JMML 4) is shown. Mutated nucleotides are indicated by arrows. Right panel: illustration of functional domains and mutations of U2AF35. Red arrow heads indicate hot-spot mutations at S34 and Q157 detected in the adult cases.[10] Blue arrow head indicates the missense mutation at R156. (**b**) Left panel: sequence chromatogram of a 6-bp in-frame deletion (c.518-523delAAGTCC) in *SRSF2* detected in JMML 17 is shown. Mutated nucleotides are indicated by arrows. Right panel: illustration of functional domains and mutations of SRSF2. Red arrow head indicates hot-spot mutation at P95 frequently detected in the adult cases.[10] Blue arrow head indicates a 6-bp in-frame deletion leading to deletion of S170 and K171.

Accepted article preview online 20 February 2012; advance online publication, 2 March 2012

No mutations were identified in the 28 cases with pediatric MDS, which included 13 cases with refractory anemia with excess blasts, 5 with refractory cytopenia of childhood, 2 with Down syndrome-related MDS, 2 with Fanconi anemia-related MDS, 2 with secondary MDS and 4 with unclassified MDS. Similarly, no mutations were detected in 93 cases with *de novo* AML or in 17 with CML, as well as 19 leukemia-derived cell lines. Our previous study in adult patients showed the frequency of mutations in *U2AF35*, *SF3B1*, *ZRSR2* or *SRSF2* to be 60/155 cases with MDS without increased ring sideroblasts and 8/151 *de novo* AML patients, emphasizing the rarity of these mutations in pediatric MDS ($P<5.0\times10^{-6}$) and AML ($P<0.02$) compared with adult cases. We found mutations in two JMML cases, JMML 4 and JMML 17. JMML 4 carried a heterozygous *U2AF35* mutation (R156M), whereas JMML 17 had a 6-bp in-frame deletion (c.518-523delAAGTCC) in *SRSF2* that resulted in deletion of amino acids S170 and K171 (Figure 1). Both nucleotide changes found in *U2AF35* and *SRSF2* were neither identified in the 60 healthy volunteers nor registered in the dbSNP database (http://www.ncbi.nlm.nih.gov/projects/SNP/) or in the 1000 genomes project, indicating that they represent novel spliceosome mutations in pediatric cases.

U2AF35 is the small subunit of the U2 auxiliary factor (U2AF), which binds an AG dinucleotide at the 3′SS, and has an essential role in RNA splicing.[13] With the exception of a single A26V mutation found in a case of refractory cytopenia with multilinage dysplasia, all the U2AF35 mutations reported in adult myeloid malignancies involved one of the two hot spots within the two zinc-finger domains, S34 and Q157, which are highly conserved across species, suggesting the gain-of-function mutations.[10] In JMML 4, the R156M U2AF35 mutation affects a conserved amino acid adjacent to Q157, suggesting it may also be a gain-of-function mutation, leading to aberrant pre-mRNA splicing possibly in a dominant fashion.

SRSF2, better known as SC35, is a member of the serine/arginine-rich (SR) family of proteins.[14] SRSF2 binds to a splicing-enhancer element in pre-mRNA and has a crucial role not only in constitutive and alternative pre-mRNA splicing but also in transcription elongation and genomic stability.[14] All mutations thus far identified in adult cases exclusively involved P95 within the intervening sequence between the N-terminal RNA-binding domain and the C-terminal RS domain.[10] This region interacts with other SR proteins, again suggesting that the P95 mutation may result in gain-of-function.[10] This proline residue is thought to determine the relative orientation of the two flanking domains of SRSF2, and a substitution at this position could compromise critical interactions with other splicing factors necessary for RNA splicing to take place. In contrast, the newly identified 6-bp in-frame deletion in JMLL 17 results in two conserved amino acids, S170 and K171, within the RS domain. Although it may affect protein–protein interactions, the functional significance of this deletion remains elusive.

JMML is a unique form of pediatric MDS/MPN characterized by activation of the RAS/mitogen-activated protein kinase signaling pathway; in 90% of cases, there are germ line and/or somatic mutations of *NF1*, *NRAS*, *KRAS*, *PTPN11* and *CBL*.[8] Although JMML shares some clinical and molecular features with CMML, its spectrum of gene mutations suggests that it is a neoplasm distinct from CMML.[15] This was also confirmed by the current results that the splicing-pathway mutations are rare in JMML, whereas they are extremely frequent (~60%) in CMML.[10] Although the two JMML cases carrying the splicing-pathway mutations had no known RAS-pathway mutations, both the pathway mutations frequently coexisted in CMML.[8]

To summarize, no mutations of *SF3B1*, *U2AF35*, *ZRSR2* or *SRSF2* are found in pediatric MDS and AML. In our study, except for *ZRSR2*, mutations were examined focusing on the reported hot spots in adult studies, raising a possibility that we may have missed some mutations occurring in other regions. However, these hot spots represent evolutionally conserved amino acids and have functional relevance, it is unlikely that the distribution of hot spots in children significantly differs from adult cases and as such, we could safely conclude that mutations of *SF3B1*, *U2AF35*, *ZRSR2* and *SRSF2* are rare in myeloid neoplasms in children. Finally, mutations of *U2AF35* and *SRSF2* may have some role in the pathogenesis of JMML, although further evaluations are required.

CONFLICT OF INTEREST

The authors declare no conflict interest.

ACKNOWLEDGEMENTS

This work was supported by Research on Measures for Intractable Diseases, Health and Labor Sciences Research Grants, Ministry of Health, Labor and Welfare, by Research on Health Sciences focusing on Drug Innovation, and the Japan Health Sciences Foundation. We would like to thank M Matsumura, M Yin, N Hoshino and S Saito for their excellent technical assistance.

J Takita[1,2], K Yoshida[3], M Sanada[3], R Nishimura[1], J Okubo[1], A Motomura[1], M Hiwatari[1], K Oki[1], T Igarashi[1], Y Hayashi[4] and S Ogawa[3]

[1]*Department of Pediatrics, Graduate School of Medicine, The University of Tokyo, Tokyo, Japan;*
[2]*Department of Cell Therapy and Transplantation Medicine, Graduate School of Medicine, The University of Tokyo, Tokyo, Japan;*
[3]*Cancer Genomics Project, Graduate School of Medicine, The University of Tokyo, Tokyo, Japan and*
[4]*Gunma Children's Medical Center, Gunma, Japan*
E-mail: sogawa-tky@umin.ac.jp

REFERENCES

1 Garcia-Manero G. Myelodysplastic syndromes: 2011 update on diagnosis, risk-stratification, and management. *Am J Hematol* 2011; **86**: 490–498.
2 Delhommeau F, Dupont S, Della Valle V, James C, Trannoy S, Masse A *et al.* Mutation in TET2 in myeloid cancers. *N Engl J Med* 2009; **360**: 2289–2301.
3 Thol F, Friesen I, Damm F, Yun H, Weissinger EM, Krauter J *et al.* Prognostic significance of ASXL1 mutations in patients with myelodysplastic syndromes. *J Clin Oncol* 2011; **29**: 2499–2506.
4 Ley TJ, Ding L, Walter MJ, McLellan MD, Lamprecht T, Larson DE *et al.* DNMT3A mutations in acute myeloid leukemia. *N Engl J Med* 2010; **363**: 2424–2433.
5 Nikoloski G, Langemeijer SM, Kuiper RP, Knops R, Massop M, Tonnissen ER *et al.* Somatic mutations of the histone methyltransferase gene EZH2 in myelodysplastic syndromes. *Nature Genet* 2010; **42**: 665–667.
6 Green A, Beer P. Somatic mutations of IDH1 and IDH2 in the leukemic transformation of myeloproliferative neoplasms. *N Engl J Med* 2010; **362**: 369–370.
7 Sanada M, Suzuki T, Shih LY, Otsu M, Kato M, Yamazaki S *et al.* Gain-of-function of mutated C-CBL tumour suppressor in myeloid neoplasms. *Nature* 2009; **460**: 904–908.
8 Perez B, Kosmider O, Cassinat B, Renneville A, Lachenaud J, Kaltenbach S *et al.* Genetic typing of CBL, ASXL1, RUNX1, TET2 and JAK2 in juvenile myelomonocytic leukaemia reveals a genetic profile distinct from chronic myelomonocytic leukaemia. *Br J Haematol* 2010; **151**: 460–468.
9 Oki K, Takita J, Hiwatari M, Nishimura R, Sanada M, Okubo J *et al.* IDH1 and IDH2 mutations are rare in pediatric myeloid malignancies. *Leukemia* 2011; **25**: 382–384.
10 Yoshida K, Sanada M, Shiraishi Y, Nowak D, Nagata Y, Yamamoto R *et al.* Frequent pathway mutations of splicing machinery in myelodysplasia. *Nature* 2011; **478**: 64–69.
11 Chen Y, Takita J, Hiwatari M, Igarashi T, Hanada R, Kikuchi A *et al.* Mutations of the PTPN11 and RAS genes in rhabdomyosarcoma and pediatric hematological malignancies. *Genes Chromosomes Cancer* 2006; **45**: 583–591.
12 Shiba N, Kato M, Park MJ, Sanada M, Ito E, Fukushima K *et al.* CBL mutations in juvenile myelomonocytic leukemia and pediatric myelodysplastic syndrome. *Leukemia* 2010; **24**: 1090–1092.

13 Zhang M, Zamore PD, Carmo-Fonseca M, Lamond AI, Green MR. Cloning and intracellular localization of the U2 small nuclear ribonucleoprotein auxiliary factor small subunit. *Proc Natl Acad Sci USA* 1992; **89**: 8769–8773.

14 Edmond V, Brambilla C, Brambilla E, Gazzeri S, Eymin B. SRSF2 is required for sodium butyrate-mediated p21(WAF1) induction and premature senescence in human lung carcinoma cell lines. *Cell Cycle* 2011; **10**: 1968–1977.

15 Emanuel PD. Juvenile myelomonocytic leukemia and chronic myelomonocytic leukemia. *Leukemia* 2008; **22**: 1335–1342.

Supplementary Information accompanies the paper on the Leukemia website (http://www.nature.com/leu)

Sequencing histone-modifying enzymes identifies UTX mutations in acute lymphoblastic leukemia

Leukemia (2012) **26,** 1881–1883; doi:10.1038/leu.2012.56

Mutations affecting epigenetic regulators have long been known to have a crucial role in cancer and, in particular, hematological malignancies.[1,2] One of the earliest epigenetic factors described altered in leukemia was the mixed lineage leukemia (*MLL*) protein which is found translocated in 10% of adult acute myeloid leukemia (AML), 30% of secondary AML and >75% of infants with both AML and acute lymphocytic leukemia (ALL). *MLL* is a SET domain-containing protein, which is recruited to many promoters and mediates histone 3 lysine 4 (H3K4) methyltransferase activity, thought to promote gene expression.[3]

In addition to *MLL* fusions, recently, somatic mutations of *UTX* (also known as *KDM6A*), encoding an H3K27 demethylase, were described in multiple hematological malignancies, including multiple myeloma and many types of leukemia cell lines.[4,5] H3K27 methylation is generally thought to cause gene repression. Complimentary to *UTX*, mutations of *EZH2*, a H3K27 methyltransferase, have been reported in both lymphoid and myeloid tumors (Figure 1).[6,7] These mutations lead to altered EZH2 activity and influence H3K27 in tumor cells. Mutations in EZH2, EED and SUZ12, which all cooperate in Polycomb repressive complex 2 have been recently described in early T-cell precursor ALL.[8] Similarly, point mutations affecting the functional jumonji C (jmjC) domain of UTX inactivates its H3K27 demethylase activity. In addition, UTX associates with MLL2 in a multiprotein complex, which promotes H3K4 methylation, and recently *MLL2* has also been found mutated in cancer, further pointing to a common and complex epigenetic deregulation in cancer.[9] In line with the growing evidence for epigenetic regulators as important in tumorigenesis, additional mutations affecting epigenetic regulators such as SETD2, a H3K36 methyltransferase, KDM3B, a H3K9 demethylase, and KDM5C, a H3K4 demethylase, have been reported and are associated with distinct gene expression patterns (Figure 1).[4]

Though the clinical significance of these findings remains to be explored, it is evident that epigenetic deregulation is having an important role in both lymphoid and myeloid leukemogenesis. Furthermore, with novel drugs at hand, such as histone deacetylase inhibitors or demethylating agents that can target and reverse epigenetic alterations, understanding the underlying molecular aberrations is of growing interest.[10] We therefore undertook an effort to examine the prevalence of somatic mutations in genes encoding histone-modifying proteins, in particular, *KDM3B*, *KDM5C*, *UTX*, *MLL2*, *EZH2* and *SETD2*, which previously were reported mutated in cancer.[4,5]

For an initial screen, we analyzed banked diagnostic primary leukemia samples from 44 childhood B-cell ALL and 50 adult AML patients, and, where available, used bone marrow samples obtained in complete remission to validate the somatic nature of the mutations. Samples had been collected with patient/parental informed consent from patients enrolled on Dana–Farber Cancer Institute protocols for childhood ALL (DFCI 00-001 (NCT00165178), DFCI 05-001 (NCT00400946)) or AML treatment protocols of the German-Austrian AML Study Group (AMLSG) for younger adults (AMLSG-HD98A (NCT00146120), AMLSG 07-04 (NCT00151242)), and the study was approved by the IRB of the participating centers.

Using conventional Sanger sequencing of primary leukemia sample-derived genomic DNA, we first screened all coding exons in which mutations have been reported previously.[4,5] Initially, we analyzed a total of 36 of 174 exons (*KDM3B* (2/24), *KDM5C* (9/26), *UTX* (7/29), *MLL2* (8/54), *EZH2* (1/20) and *SETD2* (9/21)) and found 7 non-synonymous tumor-specific aberrations. In AML, we found one *EZH2* mutation (p.G648E) in a t(8;21)-positive, and two *MLL2* missense mutations (p.R5153Q and p.Y5216S; Table 1) and one

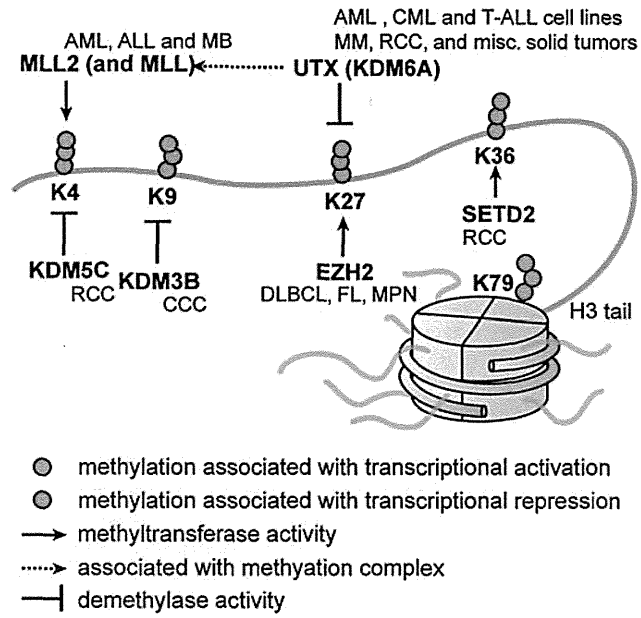

Figure 1. Histone 3 methylation and selected histone demethylases and methyltransferases. Cancers are shown in italics next to the mutated protein they are associated with. MM, multiple myeloma; FL, follicular lymphoma; DLBCL, diffuse large B-cell lymphoma; RCC, renal cell carcinoma; CCC clear cell carcinoma; MPN, myeloproliferative neoplasm; MB, medulloblastoma.

Accepted article preview online 1 March 2012; advance online publication, 3 April 2012

Journal of Receptors and Signal Transduction

http://informahealthcare.com/rst
ISSN: 1079-9893 (print), 1532-4281 (electronic)

J Recept Signal Transduct Res, 2013; 33(2): 124–128
 DOI: 10.3109/10799893.2013.779279

informa healthcare

RESEARCH ARTICLE

A novel *SOS1* mutation in Costello/CFC syndrome affects signaling in both RAS and PI3K pathways

Munkhtuya Tumurkhuu[1], Makiko Saitoh[1], Junko Takita[2,3], Yoko Mizuno[3], and Masashi Mizuguchi[1]

[1]*Department of Developmental Medical Sciences, Institute of International Health, Graduate School of Medicine,* [2]*Department of Cell Therapy and Transplantation Medicine, and* [3]*Department of Pediatrics, Faculty of Medicine, The University of Tokyo, Tokyo, Japan*

Abstract

Context: Pathological upregulation of the RAS/MAPK pathway causes Costello, Noonan and cardio–facio–cutaneous (CFC) syndrome; however, little is known about PI3K/AKT signal transduction in these syndromes. Previously, we found a novel mutation of the *SOS1* gene (T158A) in a patient with Costello/CFC overlapping phenotype. *Objective:* The aim of this study was to investigate how this mutation affects RAS/MAPK as well as PI3K/AKT pathway signal transduction.

Materials and methods: Wild-type and mutant (T158A) Son of Sevenless 1 (SOS1) were transfected into 293T cells. The levels of phospho- and total ERK1/2, AKT, p70S6K and pS6 were examined under epidermal growth factor (EGF) stimulation. *Results:* After EGF stimulation, the ratio of phospho-ERK1/2 to total ERK1/2 was highest at 5 min in mutant (T158A) SOS1 cells, and at 15 min in wild-type SOS1 cells. Phospho-AKT was less abundant at 60 min in mutant than in wild-type SOS1 cells. Phosphorylation at various sites in p70S6K differed between wild-type and mutant cells. Eighteen hours after activation by EGF, the ratio of phospho-ERK1/2 to total ERK1/2 remained significantly higher in mutant than in wild-type SOS1 cells, but that of phospho-AKT to total AKT was unchanged. *Discussion:* T158A is located in the histone-like domain, which may have a role in auto-inhibition of RAS exchanger activity of SOS1. T158A may disrupt auto-inhibition and enhance RAS signaling. T158A also affects PI3K/AKT signaling, probably via negative feedback via phospho-p70S6K. *Conclusion:* The *SOS1* T158A mutation altered the phosphorylation of gene products involved in both RAS/MAPK and PI3K/AKT pathways.

Keywords

Costello syndrome, noonan syndrome, PI3K/AKT pathway, RAS/MAPK pathway, *SOS1*

History

Received 21 January 2013
Revised 19 February 2013
Accepted 20 February 2013
Published online 26 March 2013

Introduction

Protein kinases and other messengers form highly interactive networks to achieve the integrated functions of cells. One of these critical signaling networks is a family known as rat sarcoma virus oncogene homologue (RAS)/mitogen-activated protein kinase (MAPK) cascade, which plays a major role in the regulation of embryogenesis, cell differentiation, proliferation and apoptosis (1,2).

Recently, germ-line mutations in RAS pathway genes have been recognized to cause Noonan, Costello and cardio–facio–cutaneous (CFC) syndromes (3–7). These syndromes share common clinical features, such as congenital heart defects, short stature, characteristic facial features and mental retardation. The activation of RAS is associated with its conversion from the GDP- to the GTP-bound form. Son of Sevenless 1 (SOS1) is a RAS-specific guanine nucleotide exchanger (8,9). Familial or *de novo* mutations in *SOS1* have been found in Noonan and CFC syndromes (5–7,10). Lepri et al. classified Noonan-associated *SOS1* mutations into three types: class 1 with predicted conformational rearrangements of domains, resulting in reduced enzyme auto-inhibition, class 2 with predicted enhancement of SOS1's catalytic function by membrane binding, and class 3 with mutations located in the catalytic domain (CDC25; Figure 1) (10). The mutations were inferred to disrupt auto-inhibition of RAS exchanger activity (class 1 and class 2), or to promote RAS binding to CDC25 (class 3), resulting in increased signal flow through RAS. The molecular pathogenesis of Noonan syndrome caused by a gain of function mutation in *SOS1* remains to be elucidated. A mouse carrying the *SOS1*E864K mutation shows many Noonan-like features (11). In the heart of these model mice, multiple signaling pathways are activated, including not only the RAS/MAPK pathway, but also Rac and Stat3. To better understand the pathogenesis of these syndromes, it is necessary to elucidate how various protein kinases are activated in a highly interactive network. To our knowledge, however, the activation status of the PI3K/AKT pathway in these syndromes has not been elucidated.

In a previous study, we found a novel *SOS1* mutation in a patient with Costello/CFC overlapping syndrome (12).

Address for correspondence: Makiko Saitoh, Department of Developmental Medical Sciences, Institute of International Health, Graduate School of Medicine, The University of Tokyo, Bunkyo-ku, 7-3-1, 113-0033 Tokyo, Japan. Tel: +81-3-5841-3615. Fax: +81-3-5841-3628. E-mail: makisaito-tky@umin.ac.jp

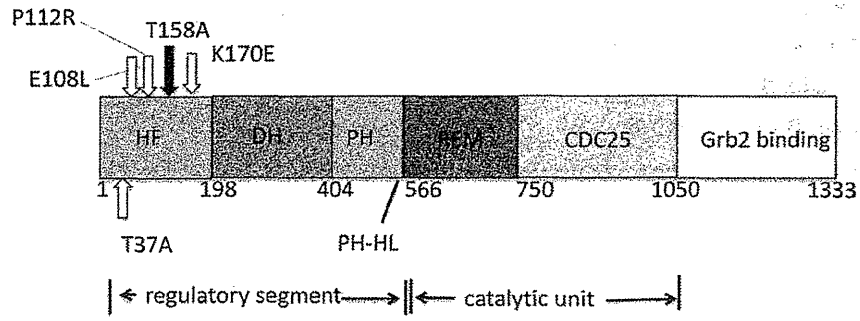

Figure 1. SOS1 domain structure and location of identified amino acid substitutions in HF domain of SOS1. The functional domains of SOS1 are as follows: DH, DBL homology; PH, pleckstrin homology; HL, helical linker; REM, RAS exchange motif; CDC25, RAS guanine nucleotide exchange factor and Grb2 binding. HF, DH, PH and HL constitute a regulatory segment, whereas REM and CDC25 form a catalytic unit. Previously reported variants in HF domain (white arrows) are K170E (class 1), E108L (class 2) and P112R (class 2). Effect of T37A on SOS1 function is unknown. T158A (black arrow) is a novel mutation found by our previous study.

This mutation caused substitution from threonine to alanine at position 158 located in the histone-like fold (HF) domain (Figure 1). This mutation is located close to a previously reported mutation K170E, which is predicted to cause conformational rearrangement of domains, resulting in reduced enzyme auto-inhibition (10). In this study, we investigated whether the *SOS1* T158A mutation can activate the RAS/MAPK pathway to cause Costello/CFC syndrome. Human embryonic kidney 293T cells were transfected with wild-type human SOS1 and mutant (T158A) isoform SOS1. Using these cells, we studied the phosphorylation of ERK1/2 and AKT under stimulation by epidermal growth factor (EGF).

Materials and methods

We expressed wild-type SOS1 and mutant T158A SOS1 in human embryonic kidney 293T cells and measured the phosphorylation level of downstream effectors of the RAS/MAPK pathway, such as extracellular signal-regulated kinase1/2 (ERK1/2), and ribosomal protein S6 (pS6), as well as that of v-Akt murine thymoma viral oncogene homolog (AKT), the main regulator of the PI3K/AKT pathway, and ribosomal protein S6 kinase, 70KDa (p70S6K). Human embryonic kidney 293T cells were maintained in Dulbecco's modified Eagle's medium (DMEM) plus 10% fetal bovine serum (FBS) and antibiotics. Human *SOS1* containing plasmid was purchased from NITE Biological Resource Center (Osaka, Japan). The primers were designed to amplify target mutation (forward: SOS1Mut1F: ATATACG GCATTATGAAATTGCAAAACAAGATAT and reverse: SOS1Mut1R: AATTTCATAATGCCGTATATTTCTTACAT AAT). We generated Costello/CFC syndrome-associated *SOS1* mutant T158A using the Gene Tailor site-directed mutagenesis system (Invitrogen, Carlsbad, CA) according to the manufacturer's protocol. Wild-type and T158A mutant plasmids were transfected into DH5αTM-T1R *Escherichia coli*. By sequencing the picked-up colonies, we confirmed the T158A mutation. Wild-type or mutant T158A *SOS1* expression constructs were transfected into 293T cells using MultiFectam reagent (Promega, Madison, WI). One day prior to transfection, the cells were plated in six-well plates at a density of 1×10^5 cells per well and were grown to 85% confluence. Plasmid DNA (2.5 μg) containing either wild-type or mutant *SOS1* was suspended with 125 μl of 20 mM Tris-HCl buffer (pH 7.4). Then, 62.5 μl MultiFectam reagent was added to the plasmid solution and was incubated for 30 min at room temperature, followed by the addition of 62.5 μl serum-free DMEM medium. For transfection, 293 T cells were incubated in this mixture for 4 h and then in complete DMEM medium with 10% FBS for 24 h. Next, for EGF stimulation, cells were cultured in DMEM without serum for 18 h. EGF (100 ng/ml medium) was then added and incubated for 5, 15 and 30 min. We determined the level of phospho-ERK1/2, phospho-pS6, phospho-AKT and phospho-p70S6K at 5, 15 and 60 min after the onset of stimulation by EGF. All the cells were scraped, collected and washed twice with phosphate-buffered saline, pH 7.4, and suspended in TS buffer (0.5 ml of 1 M Tris HCl, pH 7.7, 1.5 ml of 1 M NaCl, 1 ml of 500 mM EDTA, 7 ml distilled water containing 100 μl protease inhibitor mixture (GE Healthcare, Little Chalfont, Buckinghamshire, UK) and sonicated on ice for 15 s. The lysates were centrifuged at 12 000 g for 30 min at 4 °C, and the protein concentration of their supernatant was determined by the Bradford assay. We also examined the effect of mutant SOS1 transfection on the phosphorylation of ERK1/2 with a longer interval after EGF stimulation. The 293T cells were first stimulated by EGF in DMEM plus 10% FBS for 20 min and then cultured in serum-free DMEM for 18 h. To verify the overexpression of transfected SOS1 in 293T cells, an antibody against SOS1 (Santa Cruz Biotechnology Inc., Santa Cruz, CA) was used. ERK1/2, AKT and pS6 activations were detected by immunoblotting with antibodies against phosphorylated ERK (phospho-ERK) (Thr202/Tyr204), phosphorylated AKT (phospho-AKT) (Ser473), phosphorylated-p70S6K (phospho-p70S6K) (Thr389), phospho-p70S6K (Thr421/Ser424) and phosphorylated pS6 (phospho-pS6) (Ser235/236) purchased from Cell Signaling Technology (Beverly, MA). Band intensities were quantified using Image J software (version 1.44, NIH). For statistical analysis, data were collected from at least three independent experiments and compared using Student's *t* test. Statistical significance was determined as $p < 0.05$.

This study was approved by the Ethics Committee of the University of Tokyo.

Results

On Western blots, the 150 kDa band corresponded to the full-length SOS1. The amount of SOS1 was at least three times as high in cells transfected with mutant (T158A) SOS1 as in non-transfected cell lines (Figure 2, upper left panel). The weak SOS1 immunoreactivity of non-transfected cells

J Recept Signal Transduct Res, 2013; 33(2): 124–128

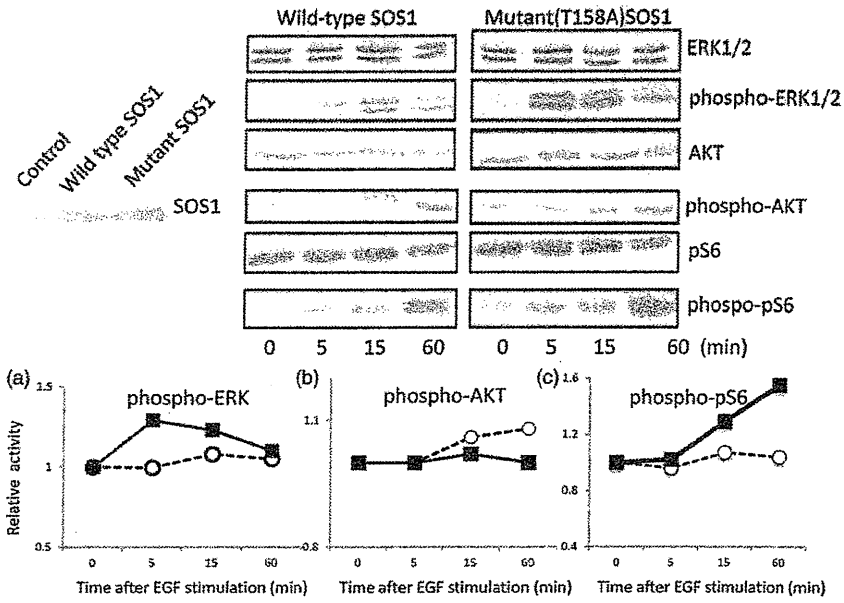

Figure 2. SOS1 T158A mutation alters early response of ERK/AKT/pS6 to EGF. The amount of the SOS1 protein was larger in cell lines overexpressing wild-type and mutant (T158A) SOS1 than in non-transfected, control cell lines (upper left panel). Upper right panels show ERK1/2, AKT and pS6 activation in cells expressing wild-type and mutant SOS1 that were starved and stimulated with EGF for 0–30 min. Lower panels show relative activity of ERK1/2, AKT and pS6 corrected by the ratio of phospho-protein to total protein at basal stage (0 min). (a) The peak of ERK1/2 phosphorylation was higher in mutant (closed square) than in wild-type SOS1 cells (open circle). (b) At 60 min, phosphorylation of AKT at was elevated in wild-type SOS1 cells, but remained unchanged in mutant cells. (c) Phosphorylation of pS6 was higher in mutant SOS1 cells than in wild-type SOS1 cells.

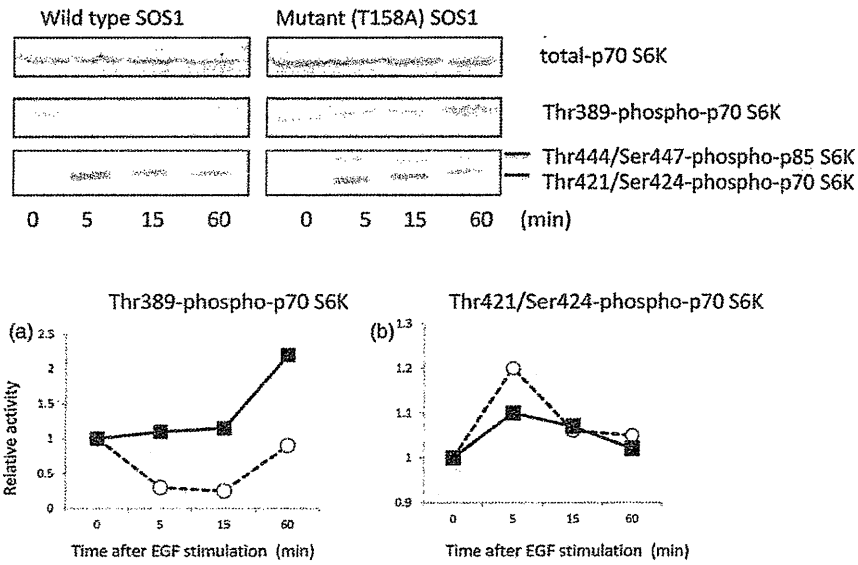

Figure 3. SOS1 T158A mutant alters the late response of p70S6K to EGF. Phosphorylation of p70S6K at various phosphorylation sites is shown in upper panel. (a) Sixty minutes after stimulation of EGF, phosphorylation of p70S6K at Thr 389 is elevated in mutant SOS1 cells. (b) Five minutes after EGF stimulation, phosphorylation of p70S6K at Thr421/Ser424 was higher in wild-type (open circle) than in mutant SOS1 cells (closed square). Phosphorylation of p85S6K at Thr444/Ser447 was detectable in mutant but not in wild-type SOS1 cells.

was considered to have resulted from endogenous expression of SOS1 protein. There was no difference between cells transfected with wild and mutated SOS1 protein.

Changes of total and phospho-ERK1/2, AKT and pS6 in 293T cells after EGF stimulation were studied by Western blotting (Figure 2, upper right panels). Western blotting of total and phospho-ERK1/2 detected 42 and 44 kDa bands, respectively. Although the basal level of phospho-ERK1/2 was low, it increased rapidly after EGF treatment (Figure 2a). The ratio of phospho-ERK1/2 to total ERK1/2 was highest 5 min after EGF stimulation in mutant SOS1 cells, while it was highest at 15 min in wild-type SOS1 cells. Phospho-AKT was barely detectable in wild-type SOS1 cells under basal conditions as well as 5 and 15 min after stimulation. Sixty minutes after stimulation, it became clearly detectable and was less abundant in mutant SOS1 cells than in wild-type SOS1 cells (Figure 2b). The increase of phospho-pS6 was more prominent and earlier in mutant SOS1 cells than in wild-type SOS1 cells (Figure 2c).

Next, to explore the reason for the effects of this mutation on AKT, we investigated the phosphorylation of p70S6K. As shown in Figure 3 (upper panel and (a)), the level of phosphorylation at Thr389 was higher in mutant SOS1 cells, but low in wild-type SOS1 cells. The phosphorylation level of Thr444/Ser447-p85S6K, an isoform of p70S6K was detectable in mutant, but not in wild-type SOS1 cells. The ratio of Thr421/Ser424-phospho-p70S6K to total-p70S6K 5 min after EGF stimulation was higher in wild-type than in mutant SOS1 cells (Figure 3b).

When the cells were starved for 18 h after stimulation by 100 ng/ml EGF, the level of phospho-ERK1/2 was significantly higher in mutant than in wild-type SOS1 cells (Figure 4, left panel), suggesting that mutant SOS1 remained active continuously, leading to higher RAS activity in

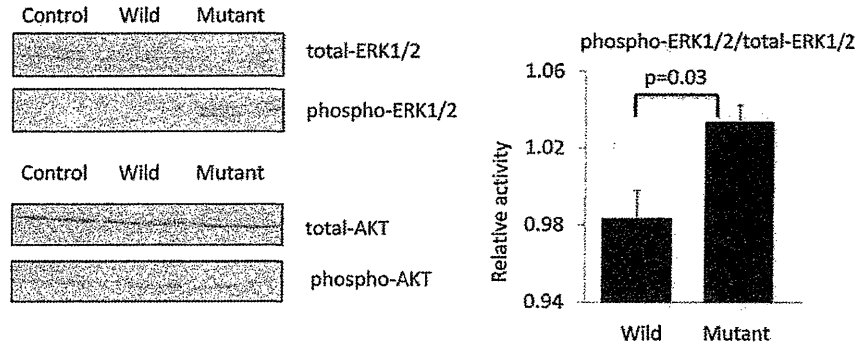

Figure 4. SOS1 T158A mutation causes prolonged activation of ERK1/2. After stimulation by EGF for 18 h, the level of phospho-ERK1/2 in the mutant SOS1 transfected cells were significantly higher than in the wild type SOS1 transfected cells, whereas that of phospho-AKT was comparable between them. The quantitative analysis (right) was based on the results of five independent experiments.

response to growth factor stimuli. The ratio of phospho- to total ERK1/2 was significantly higher in mutant than in wild-type SOS1 cells (Figure 4, right panel) ($p = 0.03$). There was no difference in the expression level of phospho-AKT 18 h after stimulation with EGF.

Discussion

In this study, we showed that *SOS1* T158A mutation causes hyper-activation of ERK1/2 in the RAS/MAPK pathway. T158A is located in the HF domain, the N-terminal segment of SOS1 that shows clear sequence similarity to histone (Figure 1). Functional analysis of mutated SOS1 with amino acid substitution in the HF domain has been reported previously (13,14). Induced mutations in the HF domain (Asp-140 and Asp-169) *in vitro* completely abolish the interaction between the isolated HF domain and other domains (14). Since the T158A mutation located in HF domain is a novel mutation that has never been reported in Costello, Noonan and CFC syndromes, we carried out a functional study to assess whether this mutation indeed alters the activation status of the RAS/MAPK pathway, as well as that of the PI3K/AKT pathway.

When we over-expressed SOS1 in 293T cells, the increase of ERK activation after EGF stimulation was faster and stronger with mutant T158A than with wild-type SOS1-transfected cells. Expression of T158A also resulted in constitutive RAS activation 18 h after EGF stimulation. Induction by EGF elicited a stronger response, both in magnitude and duration, indicating the functional consequence of the SOS1 mutation in 293T cells. These results confirmed our prediction that T158A mutation will abrogate auto-inhibition of SOS1 protein, thereby resulting in increased downstream signaling of the RAS/MAPK pathway.

The present study showed that, in the early response to EGF, phosphorylation of both ERK1/2 and p70S6K, the effectors of the RAS/MAPK pathway, was higher in mutant than in wild-type SOS1 cells. Although PI3K/AKT signaling was activated by EGF both in mutant and wild-type SOS1 cells, AKT activation was lower in mutant SOS1 cells. This finding is explained on the basis of a feedback mechanism in which activated p70S6K phosphorylates insulin receptor substrate-1 (IRS-1) to inhibit PI3K and AKT activation (15,16). The activity of p70S6K is controlled by multiple phosphorylation events located within the catalytic, linker and auto-inhibitory domains (17). Phosphorylation at Thr389 in the linker domain and at Thr421/Ser424 in the auto-inhibitory domain by mitogen-stimulated kinase in the RAS pathway precedes the activation of catalytic domain of p70S6K (17,18). In the late response to EGF, AKT activation was absent in both wild-type and mutant SOS1 cells.

The present study shows that *SOS1* T158A mutation affects both the RAS/MAPK and PI3K/AKT pathway by altering ERK and AKT phosphorylation. Activation of the RAS, PI3K, Src, PLCγ and other signaling pathways may alter cell fate after growth factor stimuli (19). To monitor their external and internal situations, cells use multiple pathways that are integrated at specific signaling steps (20,21). In PC12 cells, NGF induces combined phospho-ERK and phospho-AKT signal variation that enables a decision on differentiation and/or proliferation (22). Therefore, dysregulation in RAS/MAPK as well as PI3K/AKT signal transduction, caused by T158A SOS1 mutation, may affect the balance between cellular differentiation and proliferation and produce the clinical phenotypes of Costello/CFC syndrome.

Conclusion

The *SOS1* mutation T158A causes excessive activation of the RAS/MAPK pathway, as well as attenuated activation of AKT, in response to EGF stimulation. Altered signal transduction in the RAS/MAPK as well as PI3K/AKT pathway may account for the variable clinical expression of overlapping syndromes of the RAS/MAPK pathway.

Declaration of interest

The authors report no conflicts of interest.

Supported in part by Grants-in-Aid for Scientific Research from the Japan Society for the Promotion of Science (Nos. 20390293 and 22659190), and by a Grant-in-Aid for research (H23-Nanji-Ippan-31) from the Ministry of Health, Labour and Welfare, Japan.

References

1. Barbacid M. RAS genes. Annu Rev Biochem 1987;56:779–82.
2. Downward J. Targeting RAS signalling pathways in cancer therapy. Nat Rev Cancer 2003;3:11–22.
3. Aoki Y, Niihori T, Kawame H, et al. Germline mutations in HRAS proto-oncogene cause Costello syndrome. Nat Gene 2005;37:1038–40.
4. Zenker M, Lehmann K, Schulz AL, et al. Expansion of the genotypic and phenotypic spectrum in patients with KRAS germline mutations. J Med Genet 2006;44:131–5.
5. Roberts AE, Araki T, Swanson KD, et al. Germline gain-of-function mutations in SOS1 cause Noonan syndrome. Nat Genet 2007;39:70–4.

6. Tartaglia M, Pennacchio LA, Zhao CY. Gain-of-function SOS1 mutations cause a distinctive form of Noonan syndrome. Nat Genet 2007;39:75–9.
7. Narumi Y, Aoki Y, Niihori T, et al. Clinical manifestations in patients with SOS1 mutations range from Noonan syndrome to CFC syndrome. J Hum Genet 2008;53:834–41.
8. Boriack-Sjodin PA, Margarit SM, Bar-Sagi D, Kuriyan J. The structural basis of the activation of Ras by Sos. Nature 1998;394: 337–43.
9. Schlessinger J. Cell signaling by receptor tyrosine kinases. Cell 2000;103:211–25.
10. Lepri F, De Luca A, Stella L, et al. SOS1 mutations in Noonan syndrome: molecular spectrum, structural insights on pathogenic effects, and genotype-phenotype correlations. Hum Mut 2011;32: 760–72.
11. Chen PC, Wakimoto H, Conner D, et al. Activation of multiple signaling pathways causes developmental defects in mice with a Noonan syndrome-associated Sos1 mutation. J Clin Invest 2010; 120:4353–65.
12. Tumurkhuu M, Saitoh M, Sato A, et al. A comprehensive genetic analysis of overlapping syndromes of RAS/RAF/MEK/ERK pathway. Pediatr Int 2010;52:557–62.
13. Sondermann H, Soisson SM, Bar-Sagi D, Kuriyan J. Tandem histone folds in the structure of the N-terminal segment of the RAS activator Son of Sevenless. Structure 2003;11: 1583–93.
14. Sondermann H, Soisson SM, Boykevicsh M, et al. Structural analysis of autoinhibition in the RAS activator Son of Sevenless. Cell 2004;119:393–405.
15. Bilanges B, Vanhaesebroeck B. A new tool to dissect the function of p70 S6 kinase. Biochem J 2011;431:e1–3.
16. Harrington LS, Findlay GM, Gray A, et al. The TSC1-2 tumor suppressor controls insulin–PI3K signaling via regulation of IRS proteins. J Cell Biol 2004;166:213–23.
17. Pullen N, Dennis PB, Andjelkovic M, et al. Phosphorylation and activation of $p70^{s6k}$ by PDK1. Science 1998;279:707–10.
18. Dennis PB, Pullen N, Pearson RB, et al. Phosphorylation sites in the autoinhibitory domain participate in p70S6K activation loop phosphorylation. J Biol Chem 1998;273:14845–52.
19. Lemmon MA, Schlessinger J. Cell signaling by receptor tyrosine kinases. Cell 2010;141:1117–34.
20. Albert R. Scale-free networks in cell biology. J Cell Sci 2005;118: 4947–57.
21. Barabasi AL, Oltvai ZN. Network biology: understanding the cell's functional organization. Nat Rev Genet 2004;5:101–13.
22. Chen JY, Lin JR, Cimprich KA, Meyer T. A two-dimensional ERK-AKT signaling code for an NGF-triggered cell-fate decision. Mol Cell 2012;45:196–209.
23. Ko JM, Kim JM, Kim GH, Yoo HW. PTPN11, SOS1, KRAS, and RAF1 gene analysis, and genotype-phenotype correlation in Korean patients with Noonan syndrome. J Hum Genet 2008;53: 999–1006.